J Neurophysiol 118: 1270–1291, 2017.
First published May 31, 2017; doi:10.1152/jn.00116.2017.

RESEARCH ARTICLE | *Neural Circuits*

Mesoscale-duration activated states gate spiking in response to fast rises in membrane voltage in the awake brain

Annabelle C. Singer,[1,2]* Giovanni Talei Franzesi,[2]* Suhasa B. Kodandaramaiah,[2,3] Francisco J. Flores,[4,5] Jeremy D. Cohen,[6] Albert K. Lee,[6] Christoph Borgers,[7] Craig R. Forest,[8] Nancy J. Kopell,[9] and Edward S. Boyden[2]

[1]*Coulter Department of Biomedical Engineering, Georgia Institute of Technology and Emory University, Atlanta, Georgia;* [2]*Media Laboratory and McGovern Institute for Brain Research, Departments of Biological Engineering and Brain and Cognitive Sciences, Massachusetts Institute of Technology, Cambridge, Massachusetts;* [3]*Department of Mechanical Engineering, University of Minnesota, Twin Cities, Minneapolis, Minnesota;* [4]*Department of Brain and Cognitive Sciences, Massachusetts Institute of Technology, Cambridge, Massachusetts;* [5]*Department of Anesthesia, Critical Care and Pain Medicine, Massachusetts General Hospital and Harvard Medical School, Boston, Massachusetts;* [6]*Howard Hughes Medical Institute, Janelia Research Campus, Ashburn, Virginia;* [7]*Department of Mathematics, Tufts University, Medford, Massachusetts;* [8]*George W. Woodruff School of Mechanical Engineering, Georgia Institute of Technology, Atlanta, Georgia; and* [9]*Department of Mathematics and Statistics, Boston University, Boston, Massachusetts*

Submitted 22 February 2017; accepted in final form 29 May 2017

Singer AC, Talei Franzesi G, Kodandaramaiah SB, Flores FJ, Cohen JD, Lee AK, Borgers C, Forest CR, Kopell NJ, Boyden ES. Mesoscale-duration activated states gate spiking in response to fast rises in membrane voltage in the awake brain. *J Neurophysiol* 118: 1270–1291, 2017. First published May 31, 2017; doi:10.1152/jn.00116.2017.—Seconds-scale network states, affecting many neurons within a network, modulate neural activity by complementing fast integration of neuron-specific inputs that arrive in the milliseconds before spiking. Nonrhythmic subthreshold dynamics at intermediate timescales, however, are less well characterized. We found, using automated whole cell patch clamping in vivo, that spikes recorded in CA1 and barrel cortex in awake mice are often preceded not only by monotonic voltage rises lasting milliseconds but also by more gradual (lasting tens to hundreds of milliseconds) depolarizations. The latter exert a gating function on spiking, in a fashion that depends on the gradual rise duration: the probability of spiking was higher for longer gradual rises, even when controlled for the amplitude of the gradual rises. Barrel cortex double-autopatch recordings show that gradual rises are shared across some, but not all, neurons. The gradual rises may represent a new kind of state, intermediate both in timescale and in proportion of neurons participating, which gates a neuron's ability to respond to subsequent inputs.

NEW & NOTEWORTHY We analyzed subthreshold activity preceding spikes in hippocampus and barrel cortex of awake mice. Aperiodic voltage ramps extending over tens to hundreds of milliseconds consistently precede and facilitate spikes, in a manner dependent on both their amplitude and their duration. These voltage ramps represent a "mesoscale" activated state that gates spike production in vivo.

network state; CA1; hippocampus; barrel cortex; intracellular recording; action potential; subthreshold dynamics

A WIDE VARIETY OF DISCRETE or slowly varying (i.e., over timescales of seconds) neural network states have been observed in the living mammalian brain, with many neurons in the network participating (Haider et al. 2006; McGinley et al. 2015a, 2015b; Reimer et al. 2014; Steriade et al. 1993, 2001; Zagha and McCormick 2014). Fast dynamics occurring over timescales of a few to 10 ms have also been studied in their relationship to spike generation and timing within single neurons (Azouz and Gray 2000, 2008; Mainen and Sejnowski 1995; Nowak et al. 1997; Pouille and Scanziani 2001; Poulet and Petersen 2008). In between such slow and fast timescale events, there has been much interest in oscillations with periods in the tens to hundreds of milliseconds (e.g., Başar et al. 2001; Buzsáki and Draguhn 2004; Fries 2009; Klimesch 1999; Singer 1993).

An open question is whether there are other stereotyped forms of dynamics that help shape neural activity over intermediate timescales. We intracellularly recorded, in awake mice, spontaneous activity in the CA1 field of the hippocampus and in the barrel cortex, and discovered that most spikes were preceded by membrane voltage rises lasting tens to hundreds of milliseconds. Such voltage rises did not, however, exhibit apparent periodicity, in contrast to the oscillatory dynamics often studied over such timescales.

We characterized these intermediate duration (or mesoscale) rises in the mouse barrel cortex using simultaneous dual whole cell patch clamp (which can be performed in surface structures by our multineuron autopatching system) and found that, for any pair of neurons, they occurred in a coordinated fashion at least part of the time, suggesting that they are shared by time-varying subsets of neurons within the network. Thus these

* A. C. Singer and G. T. Franzesi contributed equally to this work.

Address for reprint requests and other correspondence: E. S. Boyden, Depts. of Biological Engineering and Brain and Cognitive Sciences, Massachusetts Institute of Technology, E15-421, 20 Ames St., Cambridge, MA 02139 (e-mail: esb@media.mit.edu).

mesoscale rises in membrane voltage appear to represent a novel activated state, intermediate both in timescale and in the proportion of neurons participating, to classical slowly varying states and fast single-neuron dynamics. These mesoscale voltage rises exerted a gating function on subsequent inputs, in the sense that neurons were more likely to spike in response to an endogenous fast rise in voltage, or to a brief near-threshold injected current, if it was preceded by a mesoscale rise. Moreover, mesoscale rises did not simply increase the probability of spiking by depolarizing the cell, because the duration of the mesoscale rise also affected spike probability: brief current pulses delivered during mesoscale rises had significantly higher probability of resulting in a spike than pulses delivered during shorter depolarizing events that reached the same prestimulus membrane voltage. This suggests that single-cell, in addition to network-level, effects can play an important role in how such membrane voltage dynamics shape neuronal output. Such intermediate activated states may facilitate neural processing by boosting the probability that a neuron might respond to a weak input, as occurs in many sensory and cognitive processes. Our results also demonstrate the new kinds of findings that can be revealed with awake autopatching and multineuron autopatching in vivo.

MATERIALS AND METHODS

Surgical Procedures

All animal procedures were approved by the MIT Committee on Animal Care. Adult male C57BL/6 mice (Taconic) 8–12 wk old were anesthetized using isoflurane and placed in a stereotactic frame. The scalp was shaved, ophthalmic ointment (Puralube vet ointment; Dechra Veterinary Products) was applied to the eyes, and Betadine and 70% ethanol were used to sterilize the surgical area. Three self-tapping screws (F000CE094; J.I. Morris) were attached to the skull, target craniotomy sites were marked on the skull [in mm, from bregma: 2 anterior/posterior (A/P), −1.4 medial/lateral (M/L) for the whole cell recording site in CA1 and −3.23 A/P, −0.58 M/L for the local field potential (LFP) electrode site in CA1; 1 A/P, −2.8 M/L; 1 A/P, −3.2 M/L; 1.5 A/P −2.8 M/L; and 1.5 A/P, −3.2 M/L for multiple whole cell recording sites in barrel cortex] and a custom stainless steel (for hippocampal recordings on the spherical treadmill) or Delrin (for barrel cortex recordings in non-running mice) headplate was affixed using dental cement (C&B-Metabond; Parkell).

On the day of the experiment, a dental drill was used with animals under isoflurane anesthesia to open one to four craniotomies (diameter 200–400 μm) by first thinning the skull until ~100 μm thick, and then a 30-gauge needle was used to make a small aperture. The craniotomy was then sealed with a sterile silicone elastomer (Kwik-Sil; World Precision Instruments) until recording. Animals were then allowed to wake up from anesthesia.

Behavior Training and Virtual Reality Environment

For CA1 recordings, the head-fixed animals ran on an 8-in. spherical treadmill as described by Harvey et al. (2009). For 16 of 18 analyzed CA1 cells, animals ran on the spherical treadmill in a dimly lit room; for 2 cells, animals ran in a virtual reality (VR) environment. For VR environment recordings, the motion of the spherical treadmill was measured by an optical mouse and fed into VR software (Aronov and Tank 2014) running in MATLAB (version 2013b; The MathWorks). The virtual environment consisted of a linear track with two small enclosures at the ends where the animal could turn. Animals received a reward of sweetened condensed milk diluted 1:2 in water from a spout at each end of the track after visiting the other end.

Animals learned to run on the track over ~1 wk. The animals were left to recover from the surgery for 1 wk and habituated to handling for 1–2 days before behavioral training began. To acclimate to the testing environment, on the first 2 days of training the animals were placed on the spherical treadmill with the VR system off and were rewarded with undiluted sweetened condensed milk. From the third day until the end of training (typically 5–7 days), the animals were placed on the treadmill for increasing amounts of time (30 min to 2 h) running in the VR linear track. Animals were rewarded with diluted (1:2) sweetened condensed milk at the end of the linear track after traversing the length of the track.

Awake Immobilized Setup and Habituation

For cortical recordings, the animals were affixed in a custom head and body restraint setup similar to that described by Guo et al. (2014). The mice were allowed to recover for 10 days after surgical implantation of headplates before habituation to the recording setup. Habituation was carried out for 6 consecutive days with training sessions lasting 30-60 min on each day. The animals were given undiluted condensed milk at 10- to 15-min intervals during the habituation sessions.

Electrophysiology Reagents

For whole cell patching, borosilicate glass pipettes (Warner Instruments) were pulled using a micropipette puller (Flaming-Brown P97 or P2000 models; Sutter Instruments) from capillaries with 0.69- and 1.2-mm internal and outer diameters, respectively. We pulled glass pipettes with resistances between 4 and 9 MΩ and with an approximate outer diameter of ~300–400 μm at a point 1.5 mm from the tip to minimize tissue displacement and to allow for the use of small craniotomies. The intracellular pipette solution consisted of (in mM) 125 K-gluconate [with more (an additional 0–25 mM) added empirically to bring the solution to ~290 mosM, pH 7.2], 0.1 $CaCl_2$, 0.6 $MgCl_2$, 1 EGTA, 10 HEPES, 4 MgATP, 0.4 NaGTP, and 8 NaCl. For biocytin staining, 500 μM biocytin (sodium salt; Invitrogen) was added to the pipette solution. The LFP electrodes were pulled from quartz capillaries with internal and outer diameters of 0.3 and 1 mm, respectively, on a pipette puller (P2000; Sutter Instruments) to a fine tip, which was then manually broken back to a diameter of ~10 μm. For recording, the LFP electrode was filled with sterile saline.

Mapping the Target Locations in CA1

Electrodes were positioned to advance through the whole cell recording site craniotomy parallel to the coronal plane and perpendicular to the horizontal plane and to advance through the LFP recording site craniotomy at an angle 60° posterior to the coronal plane and 45° inferior to the horizontal plane. The LFP electrode was slowly advanced into the brain until clear electrophysiological signatures of the hippocampal stratum pyramidale layer were observed (theta waves ~600–1,000 μV while the animal was running, clearly distinguishable sharp-wave ripples (SWRs) during immobility, multiple spikes greater than 50 μV; Fig. 1, *A* and *B*) and then retracted 25–50 μm to make room for safe positioning of the patch pipette. A similar procedure was followed to map the putative location of the stratum pyramidale through the craniotomy to be used for whole cell patching. Although the geometrical arrangement of the two electrodes was calculated to place them within 500 μm of each other, to further ensure that both LFP and whole cell recordings were taken from the same region of CA1, we simultaneously recorded the LFP at both locations and calculated the cross-correlation between the two signals at the beginning of the first recording day (Fig. 1, *A* and *C*). The pipettes were considered adequately colocalized if the cross-correlation at zero lag was above 0.85 and if, by visually inspecting the two simultaneous traces, we could confirm that the peaks and troughs of

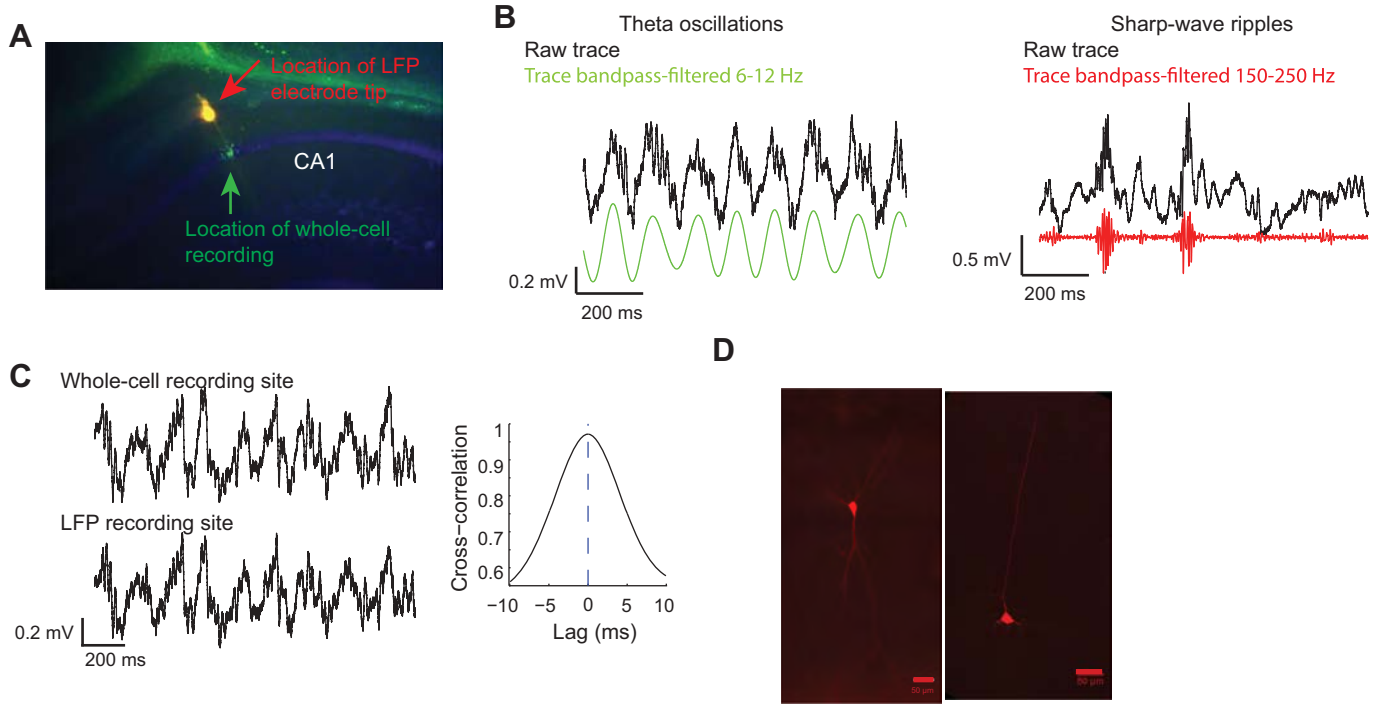

Fig. 1. Anatomical and electrophysiological validation of recordings. *A*: fluorescence micrograph of CA1 showing the location of the tip of the LFP electrode (yellow; residual DiI left by a glass electrode, indicated with red arrow), the path and final location of the patch electrode (green; whole cell recording location indicated with green arrow), and DAPI staining (blue). *B*: representative LFP recordings showing theta oscillations, with gamma oscillations nested in them [*left*; raw trace in black, bandpass-filtered (6–12 Hz) trace in green] and sharp-wave ripples [SWRs, *right*; raw trace in black, bandpass-filtered (150–250 Hz) trace in red]. C: simultaneous LFP recordings at the LFP electrode location and at the target location for whole cell recordings (*left*) and the cross-correlation between the 2 traces (*right*; >0.9 with zero lag). *D*: biocytin-filled CA1 pyramidal neuron (*left*) and biocytin-filled pyramidal neuron in barrel cortex (*right*). Scale bars, 50 μm.

theta and gamma oscillations and of SWRs were aligned within ~1 ms of each other (Fig. 1*C*). Further validation of the electrode locations was done postmortem, by either biocytin filling of patched cells or dye injection (AlexaFluor 594 and AlexaFluor 488; Molecular Probes; Fig. 1, *A* and *D*).

Awake Autopatcher Hardware and Operation

The awake autopatcher employed in our experiments was a modification of the one described by Kodandaramaiah et al. (2012). A custom-built pressure control system was used to apply positive and negative pressure to the pipette (see http://autopatcher.org). The hardware was controlled by custom software written in LabVIEW (National Instruments).

The autopatching algorithm was modified from that used in anesthetized animals to compensate for increased brain motion in awake animals. Up to the stage of gigaseal formation, the robot followed the algorithm described by Kodandaramaiah et al. (2012), with the following changes: *1*) switching to an intermediate pressure (300–800 mbar) 100 μm above the target region to minimize damage to the area of interest, *2*) advancing through the brain more slowly (2-μm steps at 1 μm/s) to give the tissue time to relax, *3*) increasing the number of samples over which to calculate resistance and *4*) using a modified threshold for cell detection (a resistance increase of 250 kΩ over 3 steps or 400 kΩ over 5 steps, with an increase of at least 50 kΩ per step) to account for movement-induced variability in the awake brain.

Gigaseal formation followed the same procedure as in Kodandaramaiah et al. (2012) but was sped up to prevent a detected cell from moving away from the pipette due to brain motion. In addition, if the resistance did not increase rapidly enough (>10 MΩ/s), the robot applied additional periods of gentle suction, moved forward 1–6 μm, and/or further hyperpolarized the pipette (up to a maximum of −90 mV). The experimenter could also manually complete patching if necessary.

Once a seal was formed (typically between 800 MΩ and several GΩ), the experimenter switched the program to break-in mode, and either sequences of suction (−150 to −250 mbar) pulses or continuous low (−20 to −30 mbar) suction was applied until whole cell access was achieved.

In addition to the changes described, keeping the craniotomy size smaller than 300 μm and using very long-shanked pipettes, to reduce tissue damage and tissue relaxation, were also important to maximize yield. Updated software for awake autopatching will be uploaded to http://autopatcher.org continuously as updates become available. Access resistances were 37.9 ± 14.6 MΩ, and membrane resistances were 93.3 ± 56.9 MΩ (means ± SD). Neurons were recorded for 16.1 ± 13.4 min (n = 61 neurons). We did not record total recording duration or membrane parameters for all neurons. Neurons were excluded from subsequent analysis if the simultaneous LFP recording was absent or contaminated by high-frequency artifacts, if the neuron did not spike at any point during the recording, or if the neuron's firing rate was above 4 Hz (see *Inclusion criteria*).

Autopatching of Two Neurons

We used four autopatchers (Kodandaramaiah et al. 2012, 2016) at once to control up to four patch pipettes simultaneously within a single cortical microcircuit. Pipettes were angled at 45° from vertical and arranged symmetrically around the craniotomies in a circle with 90° between each pipette; pipettes were 45° from the animal's midline. Pipettes were positioned in the craniotomies such that their tips entered and converged to a region 200–300 μm wide. The robot lowered all the pipettes to the target depth (350–650 μm, targeting layers 2/3, 4, and 5) and checked them for tip fouling or blockage. The robot then moved all good pipettes in small steps (2–3 μm) until a

pipette detected a neuron, whereupon the robot halted the movement of all pipettes and attempted to establish a gigaseal in the channel(s) that had encountered a neuron. After gigasealing was complete (or failed), the motor for that channel was deactivated and the rest of the pipettes resumed neuron hunting. This process was repeated until all the pipettes had encountered neurons and attempted gigasealing. At this point, the channels that had successfully formed gigaseals were selected and the robot applied pulses of suction to break into the cells for whole cell recordings. Updated software for using multiple autopatchers at once will be uploaded to http://autopatcher.org continuously as updates become available. Access resistances were 31.2 ± 15.5 MΩ, and membrane resistances were 103.9 ± 79.3 MΩ. Cells were recorded for 39.6 ± 24.6 min (n = 38 neurons). Neurons were excluded from subsequent analysis if they did not spike at any point during the recording or if the neuron's firing rate was above 4 Hz (see *Inclusion criteria*).

Data Acquisition

Data were acquired with a sampling rate of 20 kHz. LFPs were recorded simultaneously with the whole cell data at 20 kHz and bandpass filtered at 1 Hz–1 kHz. At the beginning of whole cell recording, depolarizing square-wave current pulses were delivered to measure membrane resistance, access resistance, and the membrane time constant. During some recordings, a sequence of current pulses of increasing amplitude was delivered to characterize the neuron's response properties (see e.g., Andersen 2007). Whole cell recordings in current-clamp mode then commenced. Some cells were injected with a small amount of current (0 to −100 pA) during the experiment (Epsztein et al. 2011).

We typically recorded multiple cells per animal in a session. To avoid having multiple biocytin-filled cells and to reduce background staining, we only added biocytin to pipettes to fill neurons toward the end of the recording session. Recording sessions were terminated after ~3 h for immobilized mice and ~5 h for behaving mice.

Experimental Procedures for Recordings Conducted Under Similar Conditions

Experiments were conducted in a separate laboratory at the Janelia Research Campus to determine if long ramp-ups and their gradual and fast components are present in CA1 neurons recorded by others under similar conditions (data contributed by J. D. Cohen and A. K. Lee).

Surgery. Three 8- to 12-wk-old male C57BL/6NCrl (Charles River Laboratories) mice were used for these experiments. All procedures were performed in accordance with the Janelia Research Campus Institutional Animal Care and Use Committee guidelines on animal welfare. Before behavioral training commenced, a stainless steel head plate with a large central recording well to access the hippocampus bilaterally was attached to the skull surface using light-cured adhesives (Optibond All-in-One, Kerr; Charisma, Heraeus Kulzer) and dental acrylic. Sites for future hippocampal CA1 craniotomies (bregma: −1.6 to −2.0 mm AP, 1.2 to 1.8 mm ML) were marked with a fine-tipped cautery pen (Medline). Mice were allowed to recover for at least 5 days before behavioral training started. During recovery, the mice were given food and water ad libitum.

Behavioral setup and training. The day before behavioral training started, mice were placed on water restriction (1.0 ml/day). Body weight and overall health were checked each day to ensure the mice remained healthy over the course of the experiment (Guo et al. 2014). On *day 1*, the head was centered and fixed atop a large spherical treadmill (http://www.flintbox.com/public/project/26501/), with the eyes ~20 mm from the surface. Animals received artificially sweetened water rewards (4 mM acesulfame potassium, Sigma-Aldrich; ~2-μl liquid drop per reward). Motion of the treadmill was tracked using a two-camera system (modified from https://openwiki.janelia.org/wiki/display/flyfizz/Home; Seelig et al. 2010). Over a period of 10 days, mice were trained to explore a variety of vision-based virtual reality mazes (software was developed at the HHMI Janelia Research Campus as part of Janelia's open-source virtual reality software platform, Jovian). Rewards were earned as the mice completed laps around the virtual environments.

Electrophysiology. On recording days (*day 11* and later), mice were anesthetized with isoflurane (~1.5%, ~0.8 l/min flow rate) and placed in a stereotaxic frame, and a craniotomy (~1 mm^2) was performed over dorsal CA1. A glass recording pipette (~2 MΩ) filled with saline was lowered into the brain and used to monitor the extracellular LFP and unit activity to accurately map the depth of the dorsal CA1 pyramidal cell layer. After a minimum of 1 h of postsurgery recovery time, mice were placed on the treadmill. Blind in vivo whole cell recordings were obtained from the right or left dorsal CA1 pyramidal cell layer (Lee et al. 2009, 2014) by using recording pipettes (5–7 MΩ) filled with an intracellular solution containing (in mM) 135 K-gluconate, 10 HEPES, 10 Na_2-phosphocreatine, 4 KCl, 4 MgATP, and 0.3 Na_3GTP (pH adjusted to 7.2 with KOH) as well as biocytin (0.2%). After the whole cell configuration was achieved, the VR display was turned on and the mice were free to explore the mazes for sweetened water rewards. Current-clamp measurements of membrane voltage (amplifier low-pass filter set to 5 kHz) were sampled at 25 kHz. All data analyzed are from recording periods with no holding current applied to the pipette. Recordings were not corrected for the liquid junction potential. All neurons contributed had the electrophysiological characteristics of somatic CA1 pyramidal whole cell recordings (Lee et al. 2009, 2014).

Analysis of Whole Cell Recordings

Inclusion criteria. All recorded intracellular traces were visually inspected, and only traces with a stable baseline with an average membrane voltage less than −45 mV and spike amplitude greater than 40 mV were included. Cells recorded from CA1 were also excluded if the simultaneously recorded LFP showed electrical artifacts (e.g., 60 Hz noise). We recorded 22 cells in CA1 and 25 cells in barrel cortex that reached these criteria for inclusion. Of the 25 cells recorded in barrel cortex, 8 cells were from paired recording when 2 cells were recorded simultaneously. To examine the ramp-up in voltage preceding spiking, we initially restricted the analysis to spikes that occurred at least 300 ms after a prior spike, to ensure that the ramp from baseline to spike threshold was not obscured by prior spikes. We subsequently repeated the analysis, including only spikes that occurred at least 100 ms after a prior spike, although we excluded cases when the cell did not return to baseline between spikes (e.g., bursting), obtaining quantitatively similar results.

The majority of the cells we recorded from had low mean firing rates (<4 Hz), including all but two cells in CA1 and one cell in barrel cortex. We excluded cells that had fewer than five spikes that fit our criteria for inclusion (see above). As a result, 15 cells in CA1 and 22 cells in barrel cortex were included from the single-cell analyses (details on paired recordings are described below). In these cells, more than half the spikes on average occurred at least 300 ms after a prior spike (55.13% ± 27.27% of spikes in 15 cells in CA1 and 61.11% ± 22.88% in 22 cells in barrel cortex). Greater than two-thirds of the spikes on average occurred at least 100 ms after a prior spike (66.92% ± 26.49 of spikes in CA1 and 68.30% ± 23.22 of spikes in barrel cortex).

Spike threshold calculation. In vivo, because the membrane voltage and conductance are constantly changing, spike threshold can vary by as much as 5–10 mV (Azouz and Gray 2000, 2003; Henze and Buzsáki 2001). As a result, in vivo spike threshold is often measured as the voltage reached at spike initiation, which is thought to occur at the inflection point in the membrane voltage before the spike peak (Bean 2007). To identify this inflection point, we used increases in the second derivative, specifically when the second derivative reached greater than 4 SD above the mean. This definition of spike threshold

was used for all analysis, unless otherwise noted. To confirm the robustness of our findings we also used a second definition: the highest membrane potential in the trace not associated with a spike, similar to the approach of Fontaine et al. (2014). This was calculated by finding all the times when the membrane potential went above baseline for at least 20 ms and returned to baseline without spiking, and calculating the maximum voltage during all of those periods. We called this latter method the alternate method for determining spike threshold.

Determining the start of the ramp-up. The start of the ramp-up in voltage preceding spikes was identified as the point when the membrane potential went above and stayed above the smoothed membrane potential until spike threshold (computed as described in *Spike threshold calculation*). The smoothed membrane potential was computed by first replacing spikes in the trace with a linear interpolation over 4 ms before and 7 ms after the spike peak, and smoothing the resulting trace with a 10-s-wide Gaussian filter. This produced an average of the trace without spikes that can track slow changes in voltage. We refer to this smoothed membrane potential as the baseline, for simplicity. We found quantitatively similar results if we calculated a mean baseline (the mean of the whole trace after spikes were thus removed; data not shown) instead of a smoothed membrane potential. The vast majority of the times when the membrane potential went above baseline, it peaked and returned to baseline or reached spike threshold within 400 ms; therefore, we excluded rare outliers when the membrane potential did not peak and return to baseline or reach spike threshold within this period.

Spike burst analysis. For spike burst analysis we selected spikes which were followed by another spike within 10 ms, a time window consistent with burst firing. In hippocampus, 8 cells had both single spikes and spikes separated from the next spike by less than 10 ms. In barrel cortex, 15 cells had both single spikes and spikes separated from the next spike by less than 10 ms. We found quantitatively similar results when we considered cases with a second spike within 50 ms (data not shown).

Bimodality of membrane potential traces. Hartigan's dip statistic, for which higher values indicate more bimodal distributions, was used to quantify membrane voltage bimodality. On the basis of visual inspection, distributions with a Hartigan's dip statistic less than 0.0005 were considered more unimodal, those greater than 0.001 were considered more bimodal, and those between 0.0005 and 0.001 were considered in between for purposes of being separately plotted.

Fast rise analysis. Fast, monotonic rises in membrane potential preceding spikes were calculated from the time when the slope of the membrane potential became and stayed positive until spike threshold (computed as described in *Spike threshold calculation*), meaning the membrane potential rose monotonically during that period. This definition was used for the fast rise analyses (see Figs. 4, *A–D*; 5*C*; and 7, *D–F*). To compute the slope, the despiked trace (spikes were removed and linearly interpolated over from threshold to 7 ms after the spike peak to fully remove the spike waveform) was first smoothed with a 3-ms-wide Gaussian filter, and then the change in voltage over each point in time (dV/dt) was computed. A 3-ms Gaussian was chosen for smoothing the trace before computing the slope because we found this best matched our aim of minimal smoothing that would reduce noise in the slope while accurately preserving the changes in the raw trace. Note that although such smoothing reduces our temporal resolution at durations less than 3 ms, we were not aiming to characterize dynamics in the membrane potential significantly faster than this. The size and duration of the fast rise in voltage preceding spikes was measured from the start of this positive slope. Spikes for which the fast rise in membrane potential started at or below baseline were considered to not have a gradual rise in membrane potential before threshold. Spikes that had no consistent increase in membrane potential (positive slope) before the spike were considered to have no fast rise in membrane potential before threshold.

Comparison of gradual rises and other long-lasting depolarizations. We computed the size and duration of ramp-ups above baseline that did or did not result in spikes. First, we identified depolarizing events when the membrane potential went and stayed above baseline for at least 20 ms to extract periods of depolarization that were longer than most fast rises in voltage. Next, we measured the size and duration of the ramp-up from the start of these depolarizing events to their peak if there was no spike or to spike threshold of the first spike during the event. Spikes that did not fall into one of these depolarizing events (e.g., spike threshold was at or below baseline) were rare and were excluded. We then separated ramp-ups in depolarizing events into gradual rises and fast rises, and measured the change in voltage and duration of each of these components. The end of the gradual rise and beginning of the fast rise in voltage was identified as when the slope of the membrane potential became positive and stayed positive until the peak of the event or until spike threshold.

Assessing gradual rises periodicity. To determine if gradual rises that tend to precede spikes were periodic, we measured the interval between them. To examine the periodicity of gradual rises that were similar to the depolarizing events preceding spikes, we included only those (with or without spikes) that were longer and larger than the bottom 25% of gradual rises of depolarizing events with spikes. We repeated this analysis, including only gradual rises that were longer and larger than the bottom 50% of gradual rises preceding spikes and found similar results (data not shown).

Current injection experiments. We injected in six CA1 neurons short current pulses of varying amplitudes to obtain recordings in which the neurons had a low (1.5–3.7%), medium (12–27%), or high (37–61%) probability of firing in response to the pulses. We analyzed the probability of the neurons firing in response to the stimulus as a function of the presence or absence of a gradual rise immediately preceding the current pulse (where "gradual rise" is defined as a depolarization with duration and amplitude falling within the 20th–80th percentiles of gradual rises recorded before endogenous spikes). To analyze whether gradual rises affected spike probability exclusively by bringing the membrane voltage closer to spike threshold or whether the temporal aspect of gradual rises also mattered, for each set of recordings (with low, medium, or high overall spike probability) we sorted the stimulus pulses depending on the size of the preceding depolarization (1–2, 2–5, or 5–7 mV) and its duration (0–10 and 50–200 ms). We only analyzed conditions for which >3 pulses were present and the amplitude of the prestimulus depolarization was not significantly different ($P > 0.05$) for the duration categories 0–10 and 50–200 ms. Qualitatively similar results were obtained when we analyzed the data grouping the recordings by different criteria (e.g., amplitude of evoked depolarization), having different categories for prestimulus depolarization amplitude (e.g., 1–3, 3–10 mV) and duration (e.g., 3–13, 33–95 ms).

Spike probability as a function of gradual and fast rises duration and amplitude. We binned the data by the duration or amplitude of the gradual rise and the duration or amplitude of the fast rise in voltage. For each bin, we computed the proportion of all the depolarizing events that had spikes to determine the probability of spiking as a function of the gradual rise and fast rise amplitude and duration. We computed the proportion of events with spikes per cell and then took the average of all cells. Only bins that included data from at least three cells were included.

Monotonic increases in membrane potential properties and spiking probability. We defined monotonically increasing events as events when the slope of the membrane potential became and stayed positive for at least 3 ms, to identify periods that were about the length of, or longer than, most monotonic increases preceding spikes. We then measured the size and duration to the peak of events without a spike or to spike threshold of events with a spike. As we did for the depolarizing events with spikes, we computed the proportion of monotonically increasing events with spikes as a function of the change in voltage and duration to the peak or spike threshold. We

computed the proportion of events with spikes per cell and then took the average of all cells. Only bins that included data from at least three cells were included.

Generalized linear models. To examine how the duration of the gradual rise contributed to the probability of spiking, we used a generalized linear model (GLM; Nelder and Wedderburn 1992). We first generated a logistic binomial model of the probability of spiking as a function of duration of the gradual rise alone. In this model the probability of a spike, p, was the dependent variable. The probability was predicted on the basis of the gradual rise durations of depolarizing events. Because the distribution of the dependent variable was binomial (either there was a spike in a depolarizing event or there was not), we used a binomial link function. This model is a binomial version of regression and uses the following formula, which is the canonical linking function for a binomial dependent variable: $\log [p/(1 - p)] = b_0 + b_1X_1$, where p is the probability of a spike, X_1 is the duration of the gradual rise, b_0 is the intercept, and b_1 is the coefficient of X_1. The GLM estimates b_0 and b_1 (the residuals) and yields T values and p values for those estimates that can be used to evaluate the probability that the duration of the gradual rise predicts the probability of a spike.

We looked for influential outliers using Cook's distance (Fox 2008; 10–20 points that had Cook's distances of ~0.01–0.7 that were above the other points; Cook's distance values closer to 1 are more likely to be outliers). Initially, we found some outliers, which on closer inspection were data points with long ramp-ups (greater than ~400 ms). We therefore decided to exclude cases with these extra-long ramp-ups (>300 ms). To make sure that the model was not driven by a small subset of influential points, we randomly selected half of the data and estimated the regressors with each half of the data separately. The estimates were very similar in both cases.

We then aimed to estimate the probability of spiking as a function of both the duration and size of the gradual rise. To do this, we fit a logistic binomial model of the probability of spiking as a function of duration of the gradual rise, the change in voltage during the gradual rise, and the interaction between these factors using the following linking function: $\log [p/(1 - p)] = b_0 + b_1X_1 + b_2X_2 + b_3X_1{\cdot}X_2$, where p is the probability of a spike, X_1 is the duration of the gradual rise, X_2 is the change in voltage during the gradual rise, b_0 is the intercept, b_1 is the coefficient of X_1, b_2 is the coefficient of X_2, and b_3 is the coefficient of the interaction between X_1 and X_2. Again, we looked for influential outliers using Cook's distance and found a few outliers (1–5 points that had Cook's distances of ~0.005–0.04 that were above the other points). These were all data points with larger gradual rises (greater than ~18 mV in CA1 and greater than ~26 mV in barrel cortex). We therefore decided to exclude cases with larger gradual rises (>16 mV in CA1 and >24 mV in barrel cortex). For Cook's distance, all values were less than 0.01 for single-cell analyses and less than 0.025 for paired-cell analyses.

Dual intracellular recordings analysis. The single-cell analyses included four pairs of simultaneously recorded cells. To further examine simultaneous intracellular activity, we recorded from additional cell pairs for a total of seven cell pairs in barrel cortex for which both cells reached criteria for inclusion (see *Inclusion criteria*).

In these cells we detected depolarizing events as we did for single cells. For each depolarizing event, we computed the Pearson's correlation coefficient between the membrane potential of the cells from the start of the depolarizing event until the peak of the event (if there was no spike) or until spike threshold (if there was a spike). We measured the duration and amplitude of these depolarizing events as we did for single cells, separating them into three groups: depolarizing events with a spike in the same cell used to detect the depolarizing event, with a spike in the nearby neuron but not in the same cell, or without any spikes in either cell.

We selected spikes from one cell in the pair (the reference spiking neuron) and compared the membrane potential during the period preceding those spikes with the membrane potential of the other cell in the pair (the nearby neuron). We then repeated these analysis by selecting spikes (see *Inclusion criteria*) from the other cell in the pair, which would then be deemed the spiking neuron.

Statistical analyses. We performed a Lilliefors test on each distribution to determine if it was normally distributed. When the distributions were not normal, we used appropriate nonparametric tests. When ranges of values are reported, they indicate 20th–80th percentiles unless otherwise stated.

Analysis of Local Field Potential and Network State

To detect periods of theta oscillations, SWRs, and periods outside of either network state, the LFP was first downsampled to 2 kHz and bandpass filtered between 150 and 250 Hz. SWRs were detected when the envelope amplitude of the filtered trace was greater than 4 SD above the mean for at least 15 ms. The envelope amplitude was calculated by taking the absolute value of the Hilbert transform of the filtered LFP. Spikes that occurred during the SWR and during the 250 ms before and after the ripples were classified as SWR spikes because population spiking related to SWRs (such as replay events) often extends before and after the SWR itself (Davidson et al. 2009; Dragoi and Tonegawa 2011). To detect theta periods, the LFP was bandpass filtered for theta (4–12 Hz), delta (1–4 Hz), and beta (12–30 Hz) with the use of a finite impulse response (FIR) equiripple filter. The ratio of theta to delta and beta ("theta ratio") was computed as the theta envelope amplitude divided by the sum of the delta and beta envelope amplitudes. Theta periods were classified as such when the theta ratio was greater than 1 SD above mean for at least 1 s and the ratio reached a peak of at least 2 SD above mean. SWRs and theta periods thus classified where further checked by visual inspection.

We then examined the ramp-up to spikes that occurred during theta periods, during SWR periods, or outside these periods. Twelve cells had spikes during both SWR periods and non-theta, non-SWR periods. Seven cells had spikes during both theta periods and non-theta, non-SWR periods.

Mathematical Model Describing Spike Probability as a Function of Ramp-Up Duration

Our model assumes that ramps of an arbitrary but fixed amplitude are of random duration, that spikes occur only during an ongoing ramp, and that spikes are triggered by additional random excitatory inputs arriving on a Poisson schedule with exponentially distributed inter-arrival times $\tau > 0$ with the Poisson schedule independent of the absence or presence of a ramp. Our model further assumes that a spike terminates a ramp (because this is how ramps were analyzed in the experimental data; it is difficult to analyze the ramp beyond a spike because of active conductances engaged by the spike process, so this assumption may not be correct) but that the ramp can also end without a spike.

We denote by T the random duration of a ramp that ends by itself, without a spike, and assume that T is exponentially distributed with mean $E(T) > 0$. We denote by T_R the random duration of a ramp that ends either spontaneously or with a spike, whichever occurs first: $T_R = \min(T, \tau)$. Elementary probability theory tells us that T_R is exponentially distributed with mean $E(T_R) = [1/E(T) + 1/E(\tau)]^{-1}$. With the use of elementary arguments (see Appendix), the conditional probability that a ramp ends with a spike, given that its duration T_R equals T_0 (for a given $T_0 > 0$), can be shown to equal $E(T_R)/E(\tau)$, independently of T_0. Written as a formula:

$$P\left(\text{ramp ends in a spike} \,\middle|\, T_R = T_0\right) = \frac{E(T_R)}{E(\tau)}. \quad (1)$$

RESULTS

Long Ramp-ups in Voltage Precede Spikes in CA1 Across Network and Behavior States

We recorded intracellularly from neurons in awake mice, using an awake mouse-optimized version of our automated patch-clamp robot (Kodandaramaiah et al. 2012, 2016). In neurons in hippocampal area CA1 of awake mice (Fig. 2*A*; n = 12 CA1 cells from 11 mice recorded while running on a spherical treadmill in a dimly lit room; n = 3 CA1 cells from 3 mice recorded while running on a spherical treadmill in a VR environment; see METHODS), we observed that the majority of spikes were preceded by an extended ramp-up in voltage from baseline. These ramp-ups, measured for spikes that occurred at least 300 ms after the previous spike (to standardize the analysis), lasted 31.20–114.45 ms (20th–80th percentiles; median 57.65 ms; Fig. 2, *C* and *D*) with 11.8% of the ramp-ups in CA1 neurons lasting over 150 ms. Similar results were obtained when we included spikes at least 100 ms after a prior spike: ramp-ups from baseline to threshold lasted 26.28–138.76 ms (20th–80th percentiles, median 52.50 ms for spikes that occurred 100–300 ms after a prior spike). We asked whether the long ramp-up might only occur in some specific cases, for instance, before spike bursts but not before single spikes, because these spiking patterns may be generated by different mechanisms (Grienberger et al. 2014). We therefore

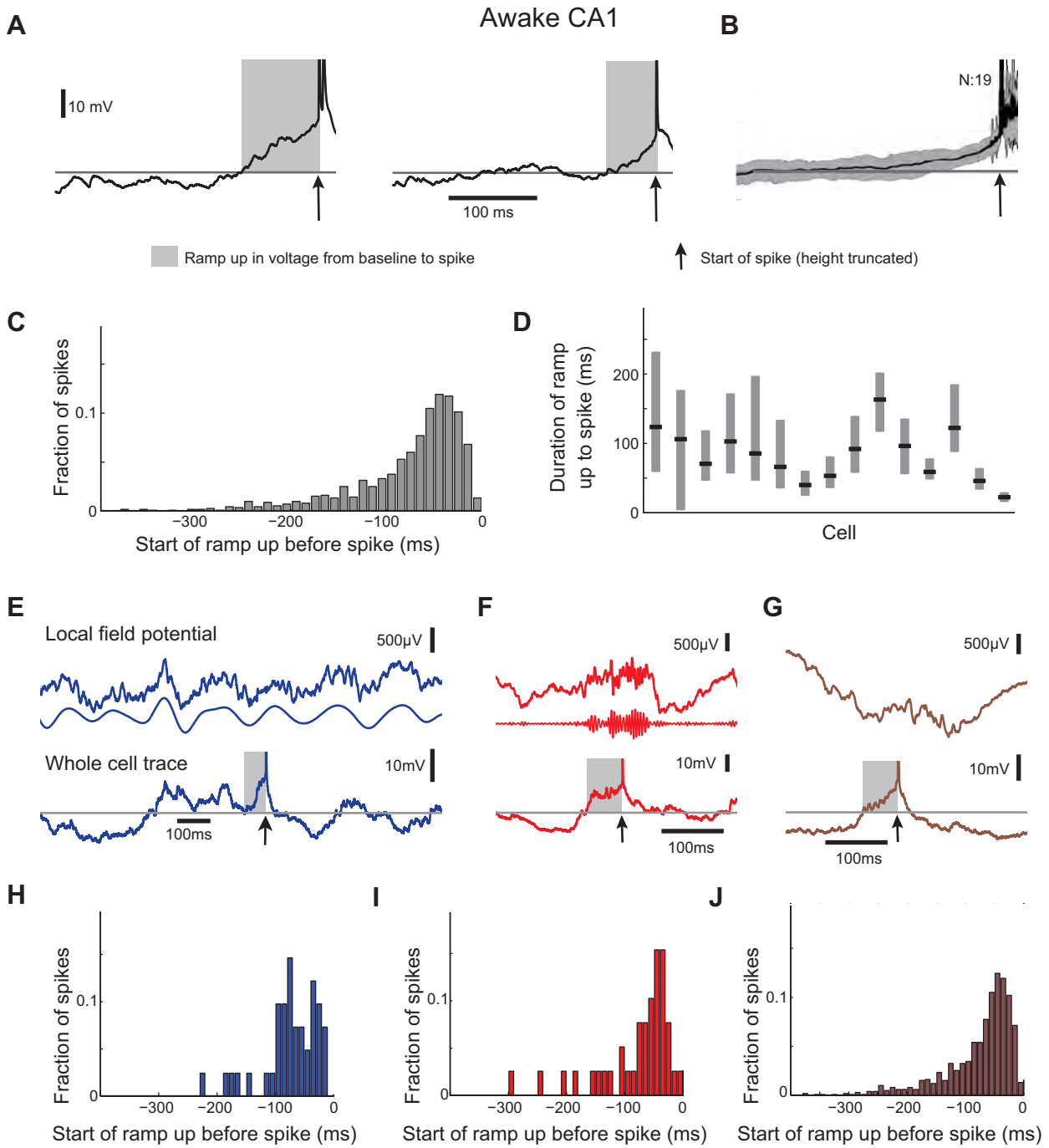

examined long ramp-ups preceding single spikes vs. multiple spikes (spikes that were followed by another spike within 10 ms, a time window consistent with burst firing; Harris et al. 2001). Spikes were preceded by long ramp-ups regardless of whether they were isolated spikes or the first spike of a burst: ramp-ups preceding multiple spikes were 19.06–95.52 ms (20th–80th percentiles, median 43.95) in duration, and those preceding single spikes were 32.66–121.06 ms (20th–80th percentiles, median 59.38) in duration. Although we found slightly shorter duration ramp-ups preceding multiple spikes compared with single spikes, in CA1 these ramp-ups were not significantly different when it was taken into account that multiple comparisons were performed (*P* values: 0.5556, 0.6625, 0.1161, 0.0214, 0.7909, 0.1538, 0.5333, and 0.2075, rank sum test, with a Bonferroni-corrected *P* value of 0.00625 for 8 CA1 cells that had both single and multiple spike events; $n = 2$–285 single spikes and 1–18 multiple spike events per cell, 20th–80th percentiles).

We then asked if long ramp-ups preceding spikes were unique to specific network states. Neural activity across the hippocampal network changes markedly when animals run vs. sit quietly, and these changes are often referred to as different network states. These network states are clearly distinguishable by the presence or absence of LFP oscillations in different frequency bands (Buzsáki 2006; Buzsáki et al. 2003). In our experiments, mice ran on a spherical treadmill while we simultaneously whole cell patched neurons and recorded the extracellular LFP to detect changes in network state in CA1 (Fig. 1*B*). When animals ran, we observed large theta (6–12 Hz) oscillations in CA1, as others have shown (Fig. 1*B*; Buzsáki 2002; Buzsáki et al. 2003; Harvey et al. 2009; Ravassard et al. 2013). When animals sat quietly, theta oscillations were no longer visible and we recorded sharp-wave ripples, high-frequency oscillations of 150–250 Hz that last around 50–100 ms and are associated with bursts of population activity, as others have observed (Fig. 1*B*; Carr et al. 2011; Foster and Wilson 2006; Ylinen et al. 1995). Long ramp-ups preceded spikes during periods of theta oscillations, sharp-wave ripples, or during periods when neither theta nor sharp-wave ripples were detected (see METHODS and Fig. 1, *A* and *B*). For spikes occurring during theta oscillations, ramp-ups started 32.85–94.26 ms before spike threshold (20th−80th percentiles, median 67.90 ms; Fig. 2, *E* and *H*); during sharp-wave ripples, ramp-ups started 36.89–116.21 ms before spike threshold (20th−80th percentiles, median 58.65 ms; Fig. 2, *F* and *I*); and during periods when neither theta nor sharp-wave ripples were detected, ramp-ups started 30.78–113.83 ms before spike threshold (20th−80th percentiles, median 56.208 ms; Fig. 2, *G* and *J*). Ramp-up durations did not differ significantly between these states (Fig. 2, *E–J*). We correlated several measures with the duration of the ramp-up in voltage preceding spikes. We found that in CA1 cells with larger differences between baseline and threshold on average, cells with lower baseline membrane potential or cells with lower firing rates tended to have longer ramp-ups (Fig. 3*A*; Pearson's linear correlation coefficient, start time of ramp-up vs. threshold: $r = -0.55$, $P = 0.033$; vs. mean baseline membrane potential: $r = 0.57$, $P = 0.028$; vs. mean firing rate: $r = 0.60$, $P = 0.019$, $n = 15$ cells in CA1). The durations of ramp-ups did not systematically depend on the degree to which the membrane voltage was unimodal or bimodal (see METHODS; Fig. 3*B*). Thus long ramp-ups occur, and exhibit similar properties, before spikes across a wide variety of cellular and network states. The hippocampal cells recorded were most likely pyramidal neurons, based on location (stratum pyramidale), low firing rate (Csicsvari et al. 1999; Hirase et al. 2001), and morphological analysis of biocytin-filled cells ($n = 3/3$ pyramidal neurons). Because we typically recorded multiple cells per animal in a session, to avoid having multiple biocytin-filled cells and to reduce background staining, we only added biocytin to pipettes to attempt to biocytin fill neurons toward the end of the recording session, so that most cells recorded were not biocytin filled.

Long Ramp-Ups Can Be Decomposed Into Slow and Fast Components

Because in vitro, in vivo, and computational studies have suggested that the last ~10 ms before a spike determine the precise timing of the spike (Azouz and Gray 2000, 2008; Mainen and Sejnowski 1995; Nowak et al. 1997; Pouille and Scanziani 2001), we examined whether a fast component at this timescale could be identified within the ramp-up. We found that the ramp-ups almost always ended in a monotonically increasing rise in membrane voltage that crossed spike threshold (Fig. 4*A*), and we developed a simple method to quantify this visual observation. This ramp-up was quite fast:

Fig. 2. Long ramp-ups in voltage precede spikes in CA1 across network and behavior states. *A*: representative traces of subthreshold activity surrounding 2 different spikes in 1 cell in CA1 with the ramp-up to spike threshold shaded in gray. Horizontal lines, baseline; black arrows, time of spike start (spike truncated). *B*: mean (black line) and SD (gray shading) of subthreshold activity surrounding spikes for the cell in *A*. Horizontal line, baseline; n = no. of spikes; black arrow, time of spike start (spike truncated). *C*: histograms of ramp-up start times relative to the time of spike threshold for CA1 neurons ($n = 15$ cells). *D*: box plots showing duration of ramp-up to spike per cell in CA1. For each cell, the median (central black mark) and 25th and 75th percentiles (top and bottom edges of filled box) are shown. *E*: representative LFP (*top*, raw trace; *middle*, bandpass-filtered for 6–12 Hz) and corresponding whole cell recording (*bottom*) when theta was detected and the cell fired. Horizontal line, baseline; black arrow, time of spike start; gray shading, ramp-up. Ramp-up durations did not differ significantly between theta and baseline (rank sum tests of ramp-up to theta vs. non-SWR, non-theta spikes with *P* values >0.2, which were greater than the Bonferroni-corrected *P* value of 0.0063 for $n = 7$ cells in CA1 that had both theta and non-SWR, non-theta spikes). *F*: representative LFP (*top*, raw trace; *middle*, bandpass-filtered for 150–250 Hz) and corresponding whole cell recording (*bottom*) during which a SWR was detected and the cell fired. Horizontal line, baseline; black arrow, time of spike start; gray shading, ramp-up. Ramp-up durations did not differ significantly between SWR and baseline (rank sum tests of ramp-up to SWR vs. non-SWR, non-theta spikes with *P* values >0.02. which were greater than the Bonferroni-corrected *P* value of 0.0042 for $n = 12$ cells in CA1 that had both SWR and non-SWR, non-theta spikes). *G*: representative LFP (*top*) and corresponding whole cell recording (*bottom*) when the cell fired and neither theta nor SWRs were detected. Horizontal black line, baseline; black arrow, time of spike start; gray shading, ramp-up. *H*: histograms of ramp-up start times relative to the time of spike threshold for spikes during theta periods in CA1 ($n = 7$ cells with spike during theta periods). *I*: histogram of ramp-up start times relative to the time of spike threshold for spikes during SWR periods in CA1 neurons ($n = 12$ cells with spikes during SWR periods). *J*: histogram of ramp-up start times relative to the time of spike threshold for spikes during periods with neither theta nor SWRs detected in CA1 ($n = 14$ cells with spikes during non-theta, non-SWR periods).

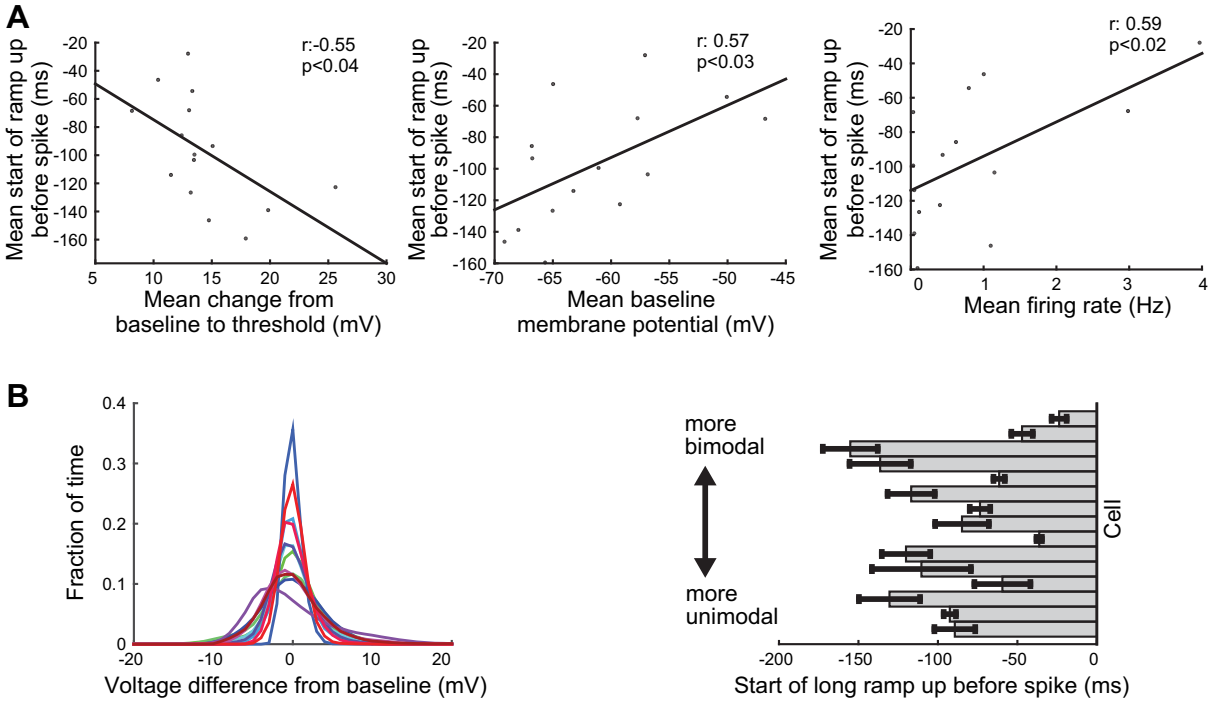

Fig. 3. Relationship between average cell properties and ramp-up duration in CA1. *A*: start time of ramp-up relative to spike time vs. mean change in membrane potential from baseline to threshold (*left*), mean baseline membrane potential (middle), and mean firing rate (*right*) for CA1 neurons (n = 15 CA1 cells). *B*: histograms of the voltage difference from baseline per cell (*left*). Each colored line is the histogram for a different cell. *Right*, mean and SD per cell of the start of the ramp-up before the spike, ordered by Hartigan's dip statistic of the membrane potential with higher values toward the *top*.

3.75–13.55 ms in duration (Fig. 4*B*; 20th-80th percentiles, median 7.40 ms). The preceding part of the ramp-up before this fast rise we called the "gradual rise" (Fig. 4*B*), which lasted almost the entire duration of the ramp-up: 22.1–105.18 ms (20–80th percentiles, median 49.93 ms, 10.53% longer than 150 ms and 1.67% longer than 250 ms, n = 15 cells). Gradual rise durations could be calculated simply by subtracting the durations of fast rises from the durations of overall long ramp-ups.

The majority of spikes were preceded by a gradual rise. Only 0.81% (median, 0–7.47% quartiles) of spikes did not have a gradual rise, and 0% (median, 0–0% quartiles, all but one cell was 0%) did not have a fast rise (n = 15; Fig. 4*D*), suggesting that both were needed to effectively fire spikes. Importantly, the vast majority of fast rises started below spike threshold, showing they are in fact a distinct component of subthreshold activity, rather than simply the initial component of spikes. We compared the starting point of the fast rise with the spike threshold, calculated according to the two spike threshold determination methods outlined (see METHODS). The vast majority of the time, the end of the gradual rise was below both measures of threshold used: only 0.71% of spikes in CA1 and 1.79% in barrel cortex reached threshold, defined as the time point when the second derivative reached greater than 4 SD above the mean (Azouz and Gray 2000, 2008; Henze and Buzsáki 2001), as a result of the gradual rise alone (that is, the "fast rise" began after the spike threshold was reached); only 0.08% of gradual rises in CA1 and 1.52% of gradual rises in barrel cortex reached above the maximum membrane potential not associated with a spike, the alternate threshold (Fontaine et al. 2014) we used. Therefore, we conclude that the voltage at the start of the fast rise in voltage was below spike threshold. The gradual rises and fast rises were similar in magnitude (Fig. 4*C*; 3.35–10.05 mV, 20th–80th percentiles, median 6.69 mV for the gradual rise vs. 3.20–8.00 mV, median 5.24 mV for the fast rise). These results held when analysis was performed with an alternate definition of spike threshold (see METHODS).

We conducted experiments in a laboratory outside of MIT to determine if long ramp-ups and their gradual and fast components are present in CA1 neurons recorded by others under similar conditions (contributed by authors J. D. Cohen and A. K. Lee; see METHODS). We found the total ramp durations in these independently recorded cells were qualitatively similar: 21.50–92.62 ms (20th–80th percentiles, median 40.08 ms, n = 3 neurons; Fig. 5, *A* and *B*). As was the case in our initial data set, we also found these long ramp-ups contained gradual and fast rises that were 14.28- to 87.40-ms gradual rises (median 36.84 ms) and 3.32- to 10.61-ms fast rises (median 6.72 ms; Fig. 5*C*). These additional data independently validate the presence of long voltage ramp-ups to spiking with gradual and fast rise components.

Gradual Rises Preceding Spikes Are Longer and Larger Than General Fluctuations in the Membrane Potential

We next examined whether gradual rises that precede spikes exhibited different properties from other long-lasting depolarizing events that do not precede spikes. We identified all of the periods where the membrane potential of a neuron rose above baseline (see METHODS for details) for at least 20 ms (a duration longer than the 80th percentile of the fast rises but shorter than the 20th percentile of the ramp-ups), decomposing each such trace into a monotonic fast rise to its peak (for depolarizations without spikes) or to spike threshold (for depolarizations with

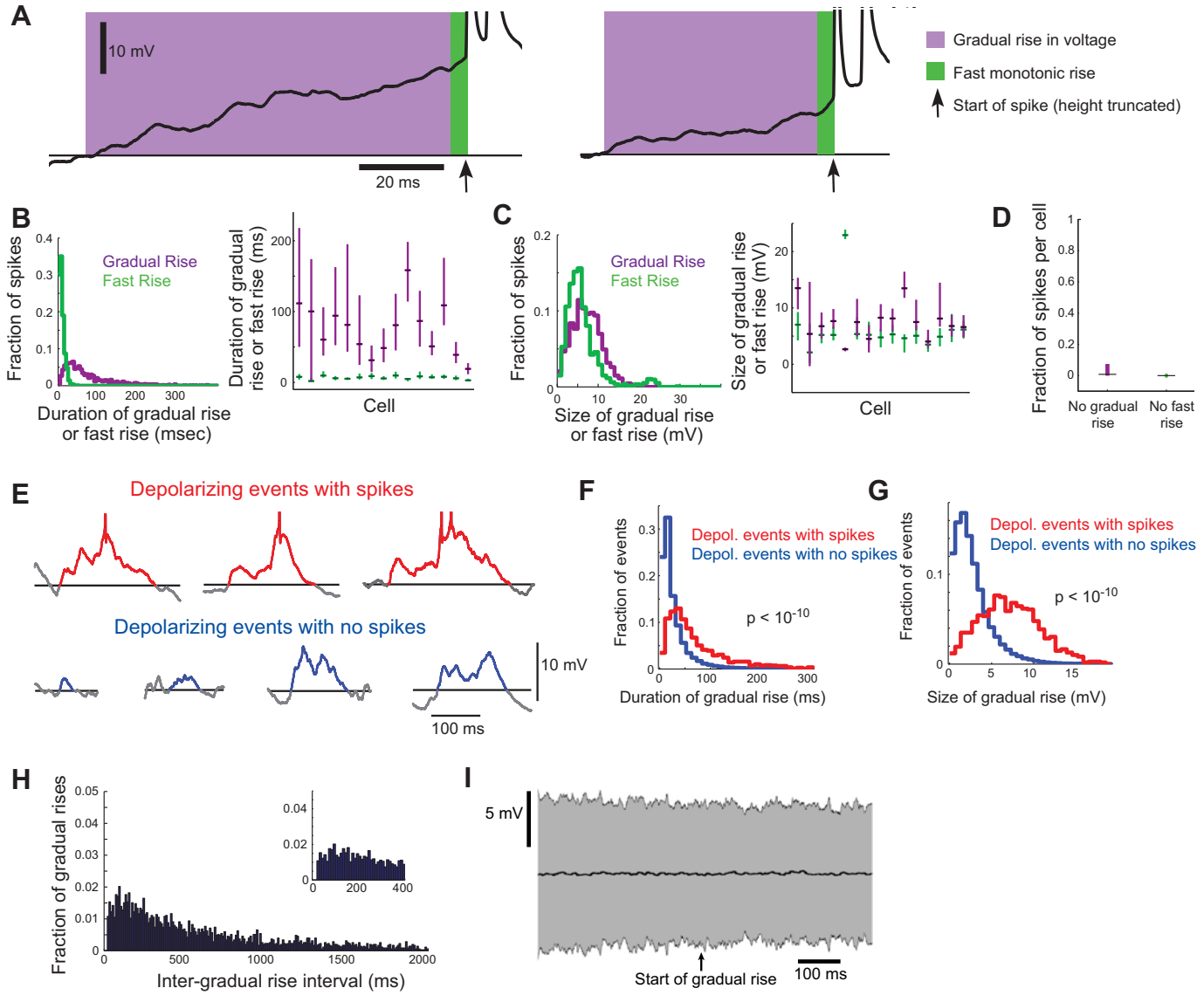

Fig. 4. Temporal properties of long-ramp-ups in voltage. *A*: representative traces of subthreshold activity surrounding spikes from 1 CA1 neuron. Horizontal black line, baseline; black arrow, time of spike start (truncated); purple shading, gradual rise in voltage; green shading, fast monotonic voltage rise. *B*: histograms of the duration of gradual rises or fast rises in voltage preceding spikes at the population level (*left*) and for each cell (*right*) in CA1 ($n = 15$ cells; gradual rises in purple, monotonic fast rises in green). Box plots (*right*) show the median (central black mark) and 25th and 75th percentiles (top and bottom edges of filled box) for each cell. *C*: histograms of the membrane potential change from baseline to the start of the fast rise in voltage and from the start of the fast rise to spike threshold at the population level (*left*) and for each cell (*right*) in CA1 ($n = 15$ cells; gradual rises in purple, monotonic fast rises in green). Box plots (*right*) show the median (central black mark) and 25th and 75th percentiles (top and bottom edges of filled box) for each cell. *D*: proportion of spikes in each cell in CA1 with no gradual rise (*left*) or no fast rise (*right*). Box plots show the median (central black mark) and 25th and 75th percentiles (top and bottom edges of filled box) for $n = 15$ cells. *E*: representative traces of depolarizing events with spikes (*top*; red) and without spikes (*bottom*; blue) in 1 CA1 neuron. Horizontal black line, baseline; gray lines, trace before and after depolarizing event. *F*: duration of gradual rises for depolarizing events with (red) and without (blue) spikes in CA1 neurons ($n = 15$ cells). *G*: magnitudes of gradual rises for depolarizing events with (red) and without (blue) spikes for CA1 neurons ($n = 15$ cells). *H*: inter-gradual rise intervals for depolarizing events with gradual rises that were typical of those that lead to spikes (larger and longer than the bottom 25% of gradual rises preceding spikes, see METHODS; $n = 15$ cells). *I*: mean (black line) and SD (gray shading) of LFP triggered by the start of depolarizing events with gradual rises that were typical of those that lead to spikes (larger and longer than the bottom 25% of gradual rises preceding spikes, see METHODS; $n = 15$ cells).

spikes), with the remaining part considered as the gradual component. Gradual rises in voltage preceding spikes were longer (Fig. 4, *E* and *F*; 26.19–113.24 ms, 20th–80th percentiles, median 52.70 ms for spike events vs. 9.50–40.01 ms, median 18.35 ms for nonspike events; $P < 10^{-50}$, rank sum test, $n = 1{,}087$ spike events and 36,217 nonspike events) and larger (Fig. 4*G*; 3.95–10.20 mV, 20th–80th percentiles, median 6.98 mV for spike events vs. 0.99–4.11 mV, median 2.21 mV for nonspike events; $P < 10^{-50}$, rank sum test) than the gradual rises of depolarizing events that did not result in spikes.

Gradual Rises Are Not Periodic and Do Not Have a Signature in the Local Field Potential

We aimed to determine if these gradual rises were related to oscillations (e.g., theta or slow oscillations) or represented a

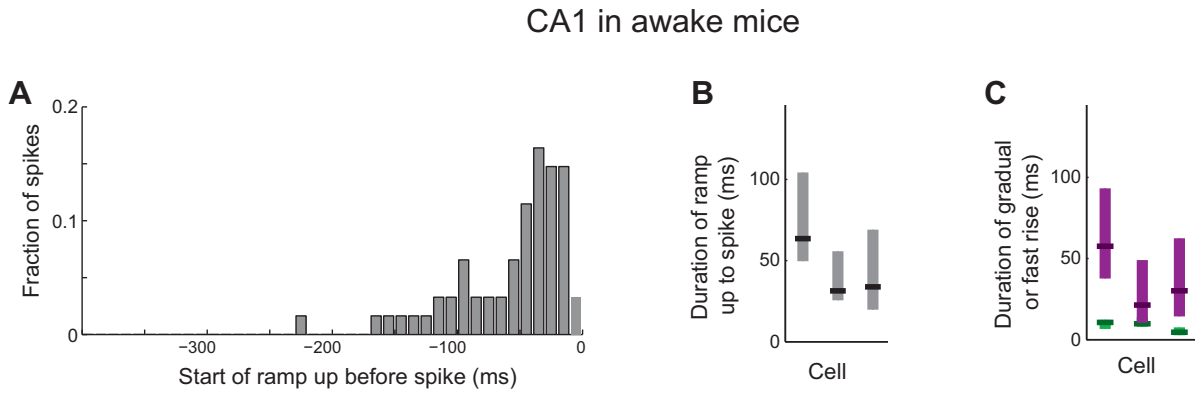

Fig. 5. Independent verification of ramp-ups. *A*: histograms of ramp-up start times relative to the time of spike threshold for CA1 neurons acquired independently ($n = 3$ cells). *B*: box plots showing duration of ramp-up to spike per cell in CA1. For each cell, the median (central black mark) and 25th and 75th percentiles (top and bottom edges of filled box) are shown. *C*: box plots of the duration of gradual rises or fast rises in voltage preceding spikes for each cell in CA1 ($n = 3$ cells; gradual rises in purple, monotonic fast rises in green). Box plots show the median (central dark mark) and 25th and 75th percentiles (top and bottom edges of filled box) for each cell.

new kind of aperiodic network phenomenon. We therefore measured the intervals between the starts of gradual rises, because an interval measure reveals if an event is periodic regardless of the shape of the trace and whether the event repeats on every period or not. Because many of the depolarizing events without spikes were short or small (see Fig. 4, *F* and *G*, distributions in blue), these small, short deviations above baseline could dominate the measure of intervals between gradual rises and might mask any potential periodicity of the large gradual rises that preferentially lead to spikes. Therefore, to examine the periodicity of gradual rises that were similar to the depolarizing events preceding spikes, we included only gradual rises of depolarizing events that were longer and larger than the bottom 25% of gradual rises of depolarizing events with spikes (see Fig. 4, *F* and *G*, 25% cutoff from distribution in red but gradual rises included from both distributions). We found a wide distribution of intervals between gradual rise onsets (180.15 ms to 1.58 s, 20th−80th percentiles, median 547.15 ms), and although there was a slight increase in gradual rise intervals between 50 and 200 ms, the majority of the intervals (81%) fell outside this range (Fig. 4*H*). We repeated this analysis, including only depolarizing events with gradual rises that were longer and larger than the bottom 50% of gradual rises preceding spikes, and found similar results. We also examined the LFP triggered from the start of these gradual rises and found no signature in the LFP to indicate extracellular oscillations (Fig. 4*I*). In all recordings (see METHODS) the distance between the two recording electrodes was <500 μm, and before each recording session we recorded LFP from both the whole cell and LFP recording sites to confirm that the LFPs were highly correlated across these locations. Recordings across both sites had a correlation coefficient of at least 0.85, and theta oscillations, gamma oscillations, and SWRs had peaks that aligned within less than a millisecond (see Fig. 1*B*). Therefore, differences between the intracellular and LFP recordings were unlikely to be due to differences in recording location. Taken together, these results not only confirm the aperiodic nature of gradual rises but additionally suggest that a smaller fraction of neurons participate in a given gradual rise compared with network states having a clear LFP signature.

Gradual Rises Gate Spiking in Response to Subsequent Inputs

To determine if monotonic increases in membrane potential alone were sufficient to determine when a cell spiked, we identified monotonically increasing events and calculated the probability of spiking as a function of their amplitude and duration (see METHODS). Perhaps surprisingly, fast rises by themselves, even when they were relatively large in amplitude, did not guarantee spiking (Fig. 6*A*), suggesting that gradual rises might play a key role in spike generation. To test this in another way, we used the patch pipette to deliver brief pulses of current to neurons in hippocampal CA1 (Fig. 6*B*, *left*). We delivered these pulses at random times and then analyzed post hoc the probability of neuron spiking as a function of whether or not it was preceded by a gradual rise (defined as a depolarizing event having length and duration in the upper 20th percentile of all depolarizing events in the population). We delivered currents that resulted in, for the no-gradual rise case, a wide variety of voltage deflections and spike probabilities; however, in all cases the presence of a gradual rise significantly enhanced the probability that the neuron would spike in response to the stimulus (Fig. 6*B*, *right*; paired-sample *t*-test, $P < 0.01$). Moreover, we aimed to determine if the duration of the gradual rise preceding the pulse affected spike probability. To control for the size of the gradual rises, we grouped current pulses by both the size and duration of the gradual rise preceding the pulse. We found that the longer the cell had been depolarized (50–200 ms compared with 0–10 ms), the higher the probability of spiking in response to the delivered current pulse, even for gradual rises of similar size (Fig. 6*C*; paired-sample *t*-test, $P < 0.05$). Note that there was a similar distribution of gradual rise sizes between short and long ramp-ups in each group. These results suggest that the duration, in addition to the amplitude, of the gradual rises is an important aspect of how these rises affect neural function. Thus gradual rises can indeed exert a causal and facilitating role on spike generation, perhaps serving as an activated state for the neuron, boosting the impact of subsequent fast events.

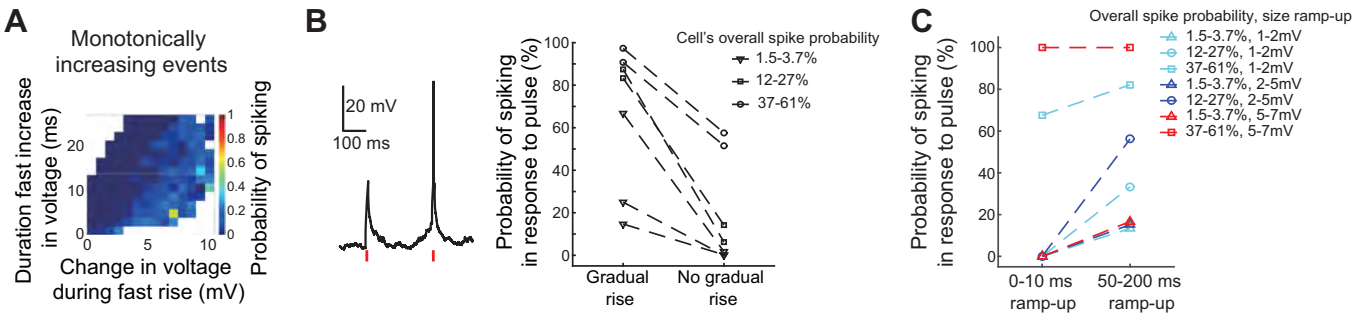

Fig. 6. Gradual rises gate spiking in response to fast inputs. *A*: probability of spiking as a function of the magnitude and duration of the fast rise of monotonically increasing events for CA1 neurons ($n = 15$ cells). *B*: example trace during pulse experiment (*left*; membrane voltage, black; time of current injection, red) and probability of spiking in response to a current pulse as a function of the presence or absence of an ongoing gradual rise (*right*). Triangles, squares, and circles denote cells where the overall probability of firing in response to a current pulse was 1.5–3.7%, 12–27%, and 37–61%, respectively (see METHODS). *C*: probability of spiking in response to a current pulse as a function of how long the cell had been depolarized by a given amount (i.e., ramp-up duration). Recordings were classified according to overall spike probability as in *B* (*right*); voltages above baseline at the time of stimulus were divided into 3 categories (1–2, 2–5, and 5–7 mV).

Long Ramp-Ups Precede Spikes In Barrel Cortex

We wondered if these long ramp-ups to spiking might be unique to the hippocampus or if they preceded spikes in neurons of other circuits, as well. To address this question, we performed whole cell patch-clamp recordings from neurons in awake mouse barrel cortex and found similar long ramp-ups preceding spikes (Fig. 7, *A–C*; 36.10–149.00 ms, 20th–80th percentiles; median 72.55 ms; $n = 22$ neurons from 15 mice that were awake, headfixed, and immobilized; see METHODS). Such long membrane voltage ramp-ups occurred before both single and multiple spikes in the hippocampus: ramp-ups preceding multiple spikes were 24.90–93.63 ms (20–80th percentiles, median 51.45) in duration, and those before single spikes were 33.29–149.27 ms (median 71.00) in duration. Only 1 cell of 14 had significantly longer ramp-ups preceding bursts when it was taken into account that multiple comparisons were performed (rank sum tests with P values of 0.2485, 0.1058, 0.7514, 0.0069, 0.0035, 0.7464, 0.9247, 0.5035, 0.0046, 0.2805, 0.1176, 0.5505, 0.6667, and 0.4206, only one of which was less than the Bonferroni-corrected P value of 0.0036 for $n = 14$ cells in barrel cortex that had both single and multiple spike events). We found similar results if we instead defined multiple spike events as cases when the spike was followed by another spike within anywhere from 6 to 50 ms, to account for the possible differences between in vitro and in vivo preparations, animal models, and recording techniques. This strongly suggests that long ramp-ups consistently precede spikes across different spiking patterns, rather than being restricted to either spike bursts or single spikes.

Average cell parameters (e.g., mean firing rate, mean change from baseline to threshold) were not correlated with ramp-up duration (Fig. 8*A*; Pearson's linear correlation coefficient, start time of ramp-up vs. mean change in membrane potential from baseline to threshold: $r = 0.18447$, $P = 0.42341$; vs. mean baseline membrane potential: $r = -0.12759$, $P = 0.58153$; and vs. mean firing rate: $r = 0.13176$, $P = 0.56915$ for $n = 21$ cells that had at least 3 spikes in barrel cortex). We also examined histograms of the voltage difference from baseline to determine if the membrane potential tended to be bimodal or unimodal. Many distributions were unimodal, whereas some were bimodal (Fig. 8*B*). We sorted the cells by the degree of bimodality or unimodality in their membrane voltage distribution, measured using Hartigan's dip statistic (Hartigan and Hartigan 1985), and found no clear relationship between the duration of the ramp-up and the degree of unimodality or bimodality of the trace (Fig. 8*B*).

These ramp-ups in barrel cortex included a gradual rise that lasted most of the ramp-up, followed by a fast rise (Fig. 7*D*; 22.67–138.56 ms, 20th–80th percentiles, median 62.4 ms, 17.57% longer than 150 ms and 5.73% longer than 250 ms; fast rise duration: 4.86–21.28 ms, 20th–80th percentiles, median 10.48 ms, $n = 22$ cells), and the fast and gradual components were of similar size (Fig. 7*E*; 3.95–14.75 mV, 20th–80th percentiles, median 10.44 mV for the gradual rise vs. 3.33–13.77 mV, median 6.54 mV for the fast rise). As in CA1, most spikes were preceded by both gradual and fast rises: only 9.22% (median, 0–21.05% quartiles) of spikes did not have a gradual rise, and 0% (median, 0–0% quartiles, all but one cell was 0%) did not have a fast rise (Fig. 7*F*; $n = 22$ cells). Furthermore, depolarizing events with spikes had longer (Fig. 7, *G* and *H*; 34.47–150.66 ms, median 72.00 ms for spike events vs. 11.00–62.67 ms, median 24.90 s for nonspike events; $P < 10^{-50}$, rank sum test, $n = 985$ spike events and 14,429 nonspike events) and larger gradual rises than depolarizing events without spikes (Fig. 7, *G* and *I*; 6.91–165.32 mV, median 11.33 mV for spike events vs. 1.61–9.14 mV, median 4.39 mV for nonspike events; $P < 10^{-50}$, rank sum test). The gradual rises in barrel cortex were also not periodic (Fig. 7*J*; gradual rise intervals were 273.90 ms to 2.02 s, 20th−80th percentiles, median 774.88 ms). These results show that long ramp-ups, consisting of a gradual rise and a fast rise, occur in multiple brain regions. We found that, as for hippocampal CA1 neurons, fast rises, even large ones, were generally unable to drive barrel cortex neurons to fire spikes (Fig. 7*K*).

Gradual Rise Properties Predict Spiking

We analyzed the probability of spiking when properties of both the gradual rise and the fast rise were considered together (Fig. 9, *A* and *C*), in recordings from both hippocampal area CA1 and barrel cortex. A diagonal pattern emerged: in general, the larger or longer the gradual rise, the smaller and shorter the fast rise needed to produce a high probability of spiking. To investigate the relationship between gradual rise duration and spike probability in the experimental data, we used a general-

ized linear model (GLM; see METHODS). We found that in the experimental data, the longer the gradual rise, the higher the probability of spiking (Fig. 9*B*, *left*, and Fig. 9*D*, *left*). The GLM derived from experimental data predicted that spikes would occur with a probability of 14.1–17.8% for CA1 neurons and 12.8–16.0% for barrel cortex neurons (95% confidence bounds) for 150-ms gradual rises, with the probability almost tripling to 42.6–55.1% for CA1 and 31.1–42.0% for barrel cortex for 250-ms gradual rises.

This result may at first not seem very surprising, because one might expect longer rises to be of higher amplitude, and one might expect higher amplitude rises to be more effective at promoting spiking. Surprisingly, however, the correlation between gradual rise duration and spiking probability holds even

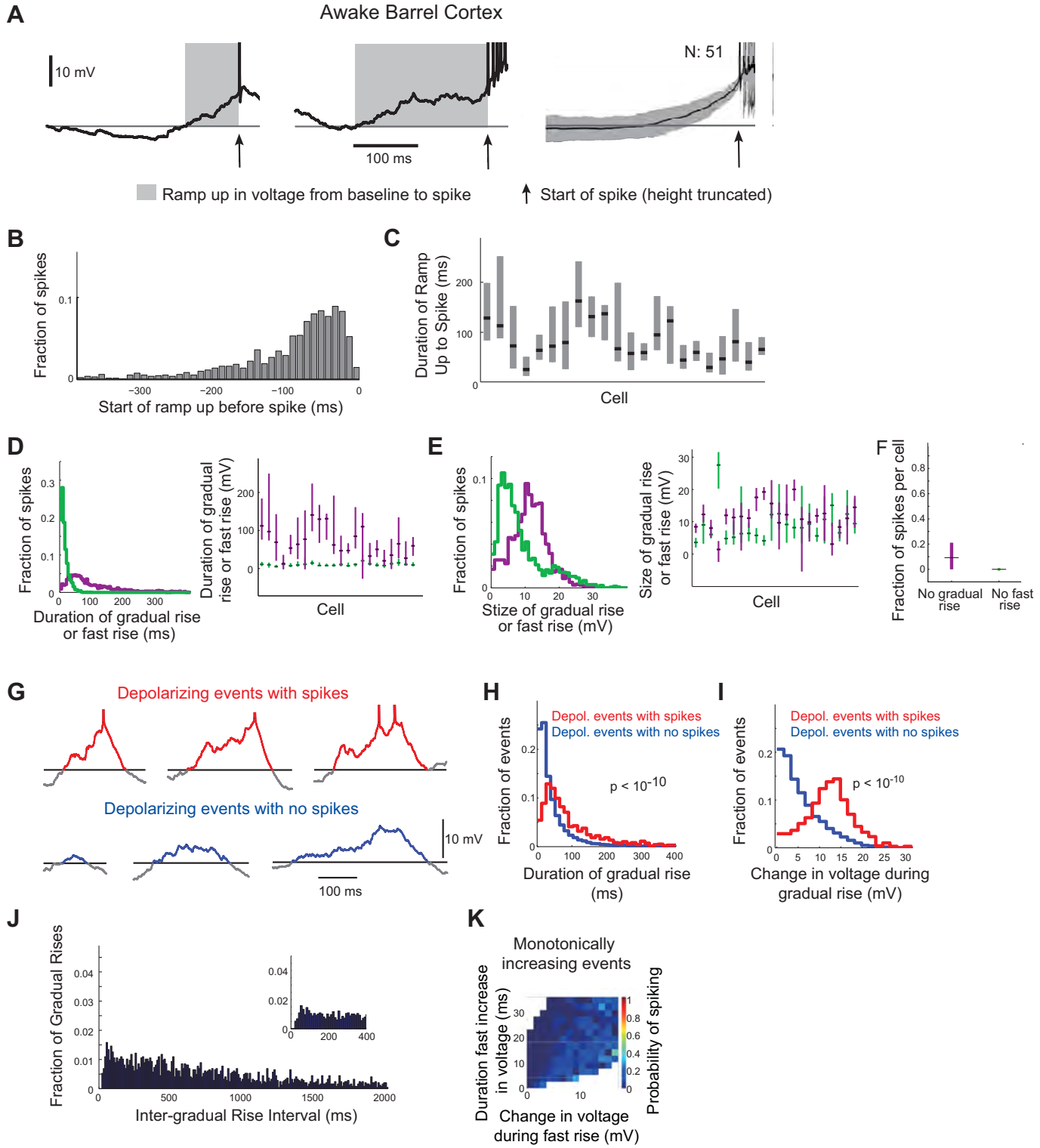

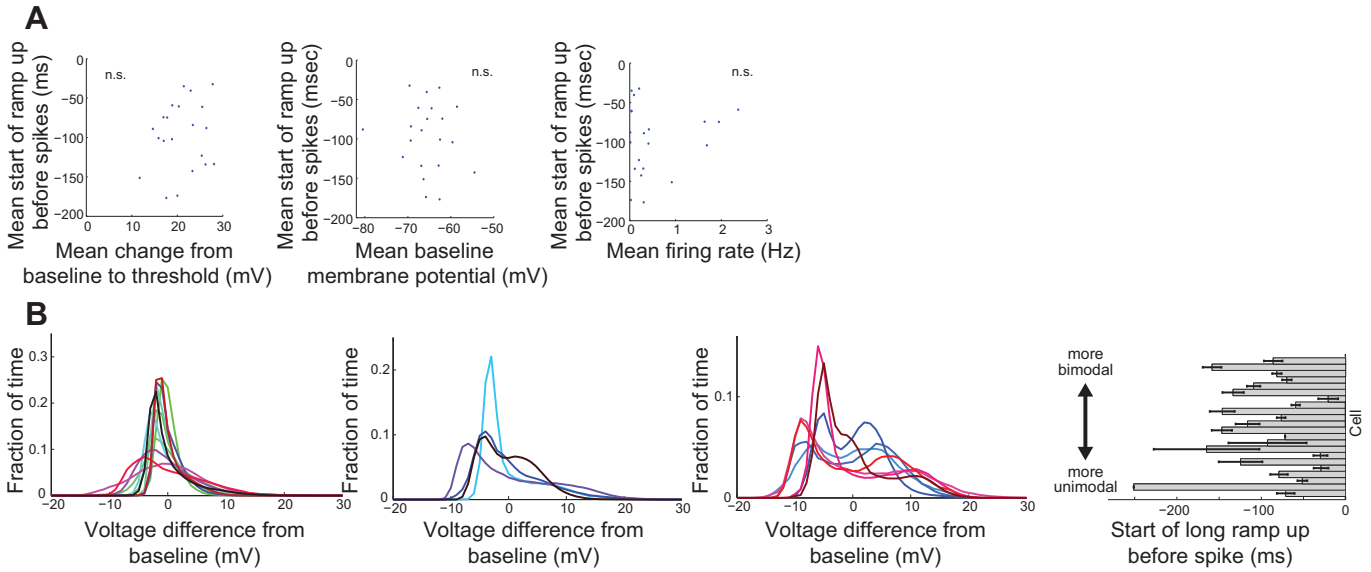

Fig. 8. Relationship between average cell properties and ramp-up duration in barrel cortex. *A*: start time of ramp-up relative to the spike time vs. mean change in membrane potential from baseline to threshold (*left*), mean baseline membrane potential (*middle*), and mean firing rate (*right*) for CA1 neurons. Cells in which there were fewer than 3 spikes total were excluded. There were no significant correlations (Pearson's linear correlation coefficient, start time of ramp-up vs. mean change in membrane potential from baseline to threshold: $r = 0.18$, $P = 0.42341$; vs. mean baseline membrane potential: $r = -0.12$, $P = 0.58153$; and vs. mean firing rate: $r = 0.13$, $P = 0.56915$; $n = 21$ cells that had at least 3 spikes in barrel cortex). *B*: histograms of the voltage difference from baseline per cell for cells with more unimodal distributions (*far left*; these had the lowest Hartigan's dip statistics, specifically <0.0005 based on visual inspection of which dip statistic cutoff seemed to best characterize unimodal or bimodal distributions), more bimodal distribution (*center right*; these had the highest Hartigan's dip statistics, specifically >0.001, again with this threshold selected on the basis of visual inspection of the distributions), and distributions that fall in between (*center left*; Hartigan's dip statistic between 0.0005 and 0.001). Each colored line is the histogram for a different cell. *Far right*, mean and SD per cell of the start of the ramp-up before the spike, ordered by Hartigan's dip statistic of the membrane potential with higher values toward the *top*. The *top* 7 bars in the bar plot correspond to the cells with the more bimodal distributions that are plotted at *center right*.

for a given maximal amplitude of the rise. In fact, including gradual rise amplitude in the model (Fig. 9*B*, *right*, and Fig. 9*D*, *right*) showed that spike probability was higher for longer duration gradual rises among gradual rises of small and medium amplitude. For instance, a 250-ms or longer gradual rise of small (4 mV) amplitude was as predictive of a spike as a much larger (12 mV), shorter rise. This shows that spike probability increases with gradual rise duration, as we also observed during artificial stimulation (Fig. 6*C*).

We asked whether this observation could be explained on purely statistical grounds, that is, whether it would be true, for probabilistic reasons alone, that long ramps would be more likely to end in a spike than short ones. A simple model (see METHODS) showed that if the ramps simply allowed spiking to occur in response to inputs by raising voltage closer to threshold (hence with constant efficacy regardless of duration), and if the fast excitatory inputs received by the neuron are Poissonian, the probability of a ramp ending in a spike would have to be independent of ramp duration, contrary to the results of the GLM.

Gradual Rises Are Coordinated Across Cells Whereas Fast Rises Are Cell Specific

The lack of a clear LFP signature suggests that not all cells in the network receive inputs underlying the gradual rises. To determine if these gradual rises are, however, coordinated across some fraction of the cells, we used a four-channel version of our autopatcher to record pairs of neurons within 500 μm of each other in the barrel cortices of awake mice. In

Fig. 7. Long ramp-ups in voltage precede spikes in barrel cortex. *A*: representative traces of subthreshold activity surrounding spikes from one barrel cortex neuron (*left*). Mean (black line) and SD (gray) of subthreshold activity surrounding spikes are shown for the same cell (*right*). Horizontal lines, baseline; n = no. of spikes; black arrows, time of spike start (spike truncated). *B*: histograms of ramp-up start times relative to the time of spike threshold for barrel cortex neurons ($n = 22$ cells). *C*: box plots showing duration of ramp-ups to spikes across cells in barrel cortex ($n = 22$ cells). For each cell, the median (central black mark) and 25th and 75th percentiles (top and bottom edges of filled box) are shown. *D*: histograms of the duration of gradual rises or fast rises in voltage preceding spikes at the population level (*left*) and for each cell (*right*) in barrel cortex ($n = 22$ cells; gradual rises in purple, monotonic fast rises in green). Box plots (*right*) show the median (central darker mark) and 25th and 75th percentiles (top and bottom edges of filled box) for each cell. *E*: histograms of the membrane potential change from baseline to the start of the fast rise in voltage and from the start of the fast rise to spike threshold at the population level (*left*) and for each cell (*right*) in barrel cortex ($n = 22$ cells; gradual rises in purple, monotonic fast rises in green). Box plots (*right*) show the median (central darker mark) and 25th and 75th percentiles (top and bottom edges of filled box) for each cell. *F*: proportion of spikes in each cell in barrel cortex with no gradual rise (*left*) or no fast rise (*right*). Box plots show the median (black) and 25th and 75th percentiles (top and bottom edges of filled box; $n = 22$ cells). *G*: representative traces of depolarizing events with spikes (*top*; red) and without spikes (*bottom*; blue) in one barrel cortex neuron. Horizontal black line, baseline; gray lines, trace before and after depolarizing event. *H*: duration of gradual rises for depolarizing events with (red) and without (blue) spikes in barrel cortex neurons ($n = 22$ cells). *I*: magnitudes of gradual rises for depolarizing events with (red) and without (blue) spikes for barrel cortex neurons ($n = 22$ cells). *J*: inter-gradual rise intervals for depolarizing events with gradual rises that were typical of those that lead to spikes (larger and longer than the bottom 25% of gradual rises preceding spikes, see METHODS; $n = 22$ cells). *Inset*: zoomed-in view of histogram. *K*: probability of spiking as a function of the magnitude and duration of the fast rise of monotonically increasing events for the barrel cortex neurons ($n = 22$ cells).

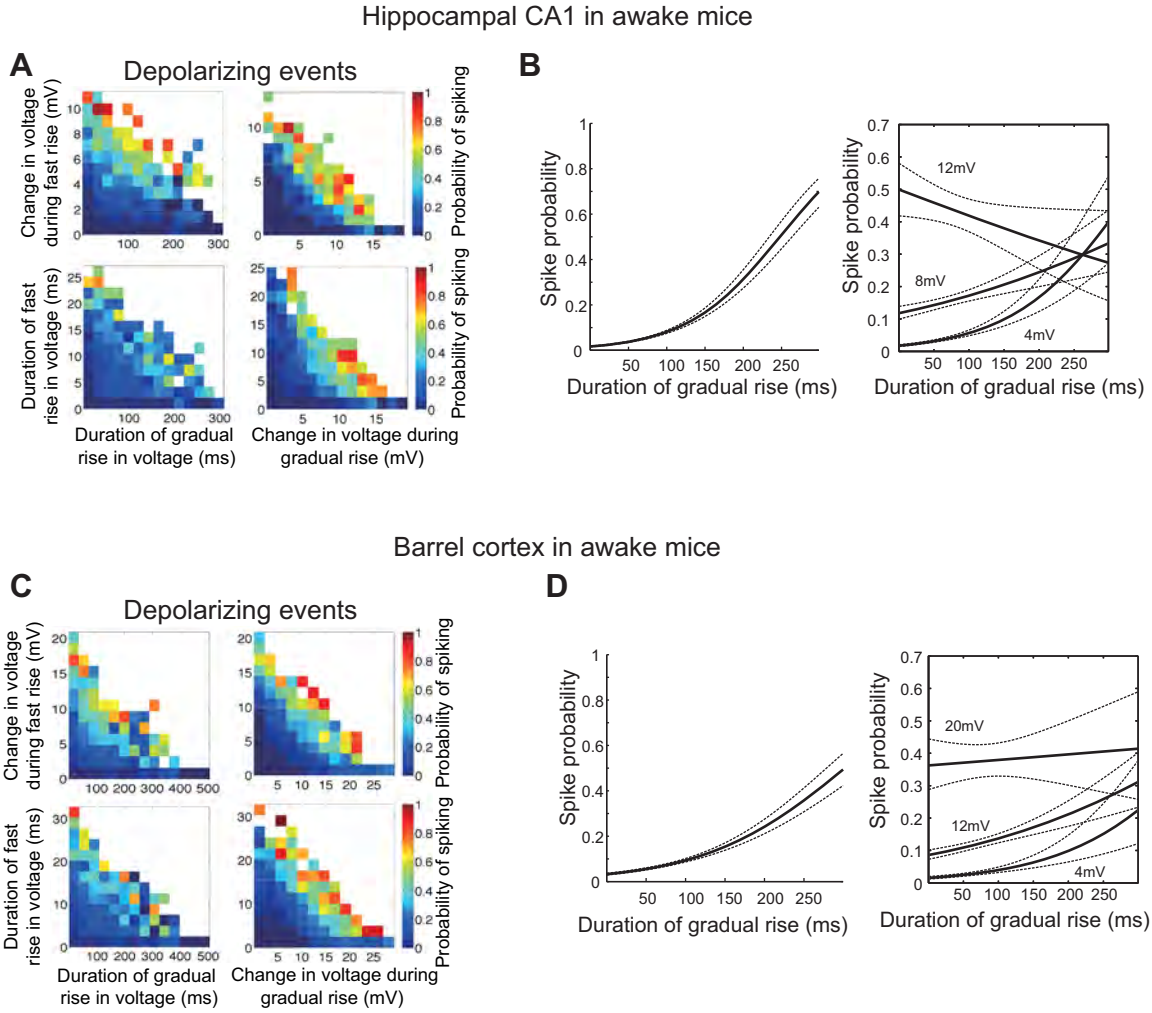

Fig. 9. Predicting spike probability from the duration and magnitude of extended depolarizing events. *A*: mean probability of spiking across cells as a function of duration (*left*) and magnitude (*right*) of the gradual rise and the magnitude (*top*) and duration (*bottom*) of the fast rise of depolarizing events for the CA1 neurons. *B*: logistic regression predicted by the general linear model of the probability of spiking as a function of the duration of the gradual rise (*left*). Slices through the logistic regression surface (*right*) predicted by the general linear model of the probability of spiking as a function of the duration and size of the gradual rise with slices at different gradual rise amplitudes. Dashed lines, 95% confidence bounds for the CA1 neurons ($n = 15$ cells). *C* and *D*: same as *A* and *B* for barrel cortex neurons ($n = 22$ cells).

seven pairs of neurons, we noted that when one neuron spiked (denoted the "reference neuron"), its ramp-up in voltage was sometimes highly correlated with the ramp-up of the other neuron (denoted the "nearby neuron"), whether the nearby neuron spiked or not. For example, in one neuron (Fig. 10*A*), 47.6% of these events exhibited a correlation greater than 0.5, whereas 12.02% of the events exhibited a correlation of less than −0.5. Thus uncorrelated as well as anticorrelated events could be observed, even in the same cell. Across all cell pairs, 7.27% of events were anticorrelated (i.e., with correlation less than −0.5), with 6 of the 7 cell pairs exhibiting at least some anticorrelated events. Overall, this suggests that gradual rises are shared across subsets of neurons in a network. However, neurons that exhibit high correlations at some times can be uncorrelated at other times so that the fraction of the network being in an activated states changes over time.

To compare ramp-ups between cells, we selected spikes from one cell in the pair (the reference spiking neuron) and compared the membrane potential during the period preceding those spikes to the membrane potential of the other cell in the pair (the nearby neuron). We then repeated these analyses, selecting spikes (see *Inclusion criteria*) from the other cell in the pair, which would then be deemed the spiking neuron. On the whole, the correlations in ramp-up were significantly larger during depolarizing events that led to spiking in at least one neuron of the pair than during depolarizing events (i.e., periods when the membrane voltage rose above baseline) that did not lead to spikes in either neuron (Fig. 10*B*; $P = 0.00021$, rank sum test; $n = 6{,}282$ depolarizing events with no spikes in either neuron and 289 depolarizing events with a spike in at least one neuron). These results show that gradual rises that lead to spikes are not only larger and longer than those that do not lead to spikes but also are more coherent across the network, providing further evidence of their identity as distinct neuronal states. To probe this further, we examined whether it was even possible to predict the spiking of one neuron using only the duration of the gradual rise exhibited by the other neuron. Perhaps surprisingly, using a GLM as in Fig. 9, *B* and *D*, we found that gradual rises lasting 250 ms in one neuron were associated with the other neuron exhibiting a 29.2%

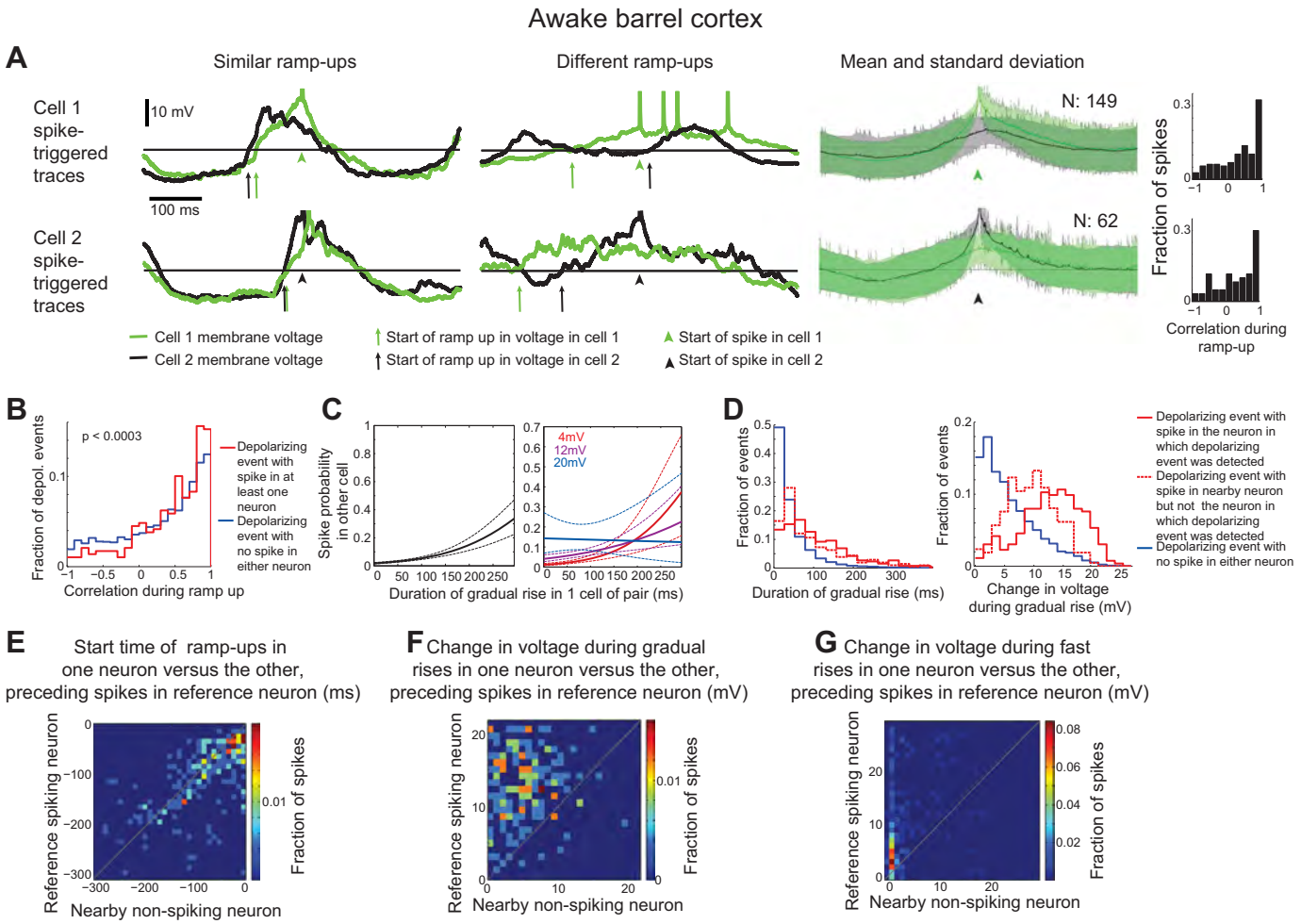

Fig. 10. Shared gradual rises and cell-specific fast rises sum toward spike generation. *A*: properties of ramp-ups in 2 simultaneously recorded neurons within 500 μm of each other in awake mouse barrel cortex. From *left* to *right*: representative traces showing ramp-ups similar in appearance; representative traces showing ramp-ups different in appearance; mean (solid line) and SD (shaded region) for all included spikes in the cells (n = 149 spikes for *cell 1*, *top*, and 62 spikes for *cell 2*, bottom); and histograms of the correlations between voltage traces in the 2 cells for each ramp-up event analyzed. In each case, data are from when *cell 1* (*top*) or *cell 2* (*bottom*) spiked. Arrowheads, time of spike start (truncated); arrows, start of ramp-up. *B*: correlation of the membrane potentials of nearby (i.e., within 500 μm) neurons during the ramp-up for depolarizing events with spikes in at least 1 cell (red; n = 289 depolarizing events) and without spikes in either cell (blue; n = 6,282 depolarizing events). *C*: logistic regression predicted by the general linear model of the probability of spiking in 1 cell as a function of the duration of the gradual rise in the other cell (*left*). Slices through the logistic regression surface (*right*) predicted by the general linear model of the probability of spiking in 1 cell as a function of the duration and size of the gradual rise in the other cell with slices at different gradual rise amplitudes (size indicated at *top left*). Dashed lines show 95% confidence bounds. *D*: duration (*left*) and change in voltage (*right*) of the gradual rise for depolarizing events with spikes (red; n = 263 depolarizing events), depolarizing events in which only the other neuron spiked (red dashed line; n = 211 depolarizing events), and events without spikes in either neuron (blue; n = 5,492 depolarizing events). Changes in voltage (*right*) were 5.96–13.10 mV (20th–80th percentiles), median 9.73 mV (dotted red line); 1.76–9.59 mV, median 4.63 mV (blue line); and 8.69–17.59 mV, median 13.32 mV (solid red line). $P < 10^{-20}$, rank sum test, depolarizing events with no spikes in either neuron vs. depolarizing events with a spike in the current neuron; $P < 10^{-20}$, rank sum test, depolarizing events with no spikes in either neuron vs. depolarizing events with no spikes in the current neuron but a spike in the nearby neuron; and $P < 10^{-10}$, rank sum test, depolarizing events with a spike in the current neuron vs. depolarizing events with no spikes in the current neuron but a spike in the nearby neuron (n = 5,492 depolarizing events with no spikes in either neuron, 263 depolarizing events with a spike in the current neuron, and 211 depolarizing events with no spikes in the current neuron but a spike in the nearby neuron). *E*: start time for ramp-ups with spikes vs. the ramp-ups in the other neuron of a recorded pair. Only cases when the nearby neuron did not spike within 150 ms of the reference neuron spike are included (n = 249 spikes). Color indicates the fraction of spikes in a bin. Gray line shows $y = x$. *F*: magnitude of gradual rises with spikes vs. gradual rises in the other neuron of a recorded pair. Only cases when the nearby neuron did not spike within 150 ms of the reference neuron spike are included (n = 249 spikes). Color indicates the fraction of spikes in a bin. Gray line shows $y = x$. *G*: magnitude of fast rises with spikes vs. fast rises in the other neuron of a recorded pair. Only cases when the nearby neuron did not spike within 150 ms of the reference neuron spike are included (n = 249 spikes). Color indicates the fraction of spikes in a bin. Gray line shows $y = x$.

chance of spiking (Fig. 10*C*, *left*). Note that this ability to predict the spiking of one neuron, from the gradual rises of the other, occurred to some extent even when the latter neuron was engaged in a depolarizing event that did not contain or result in a spike. As before, small gradual rises that were of long duration were as predictive as large gradual rises (Fig. 10*C*, *right*).

We analyzed depolarizing events that did not contain a spike but during which the other neuron did spike (Fig. 10*D*, *left*, dotted red line). These possessed gradual rises that were also larger and longer (29.49–161.37 ms, 20th–80th percentiles, median 69.35 ms vs. 12.05–66.95 ms, median 26.9 ms; $P < 10^{-20}$, rank sum test, smaller than the Bonferroni-corrected P value of 0.017 for 3 comparisons, n = 5,492 depolarizing

events with no spikes in either neuron and 211 depolarizing events with no spikes in the current neuron but a spike in the nearby neuron) than depolarizing events during which neither neuron spiked (Fig. 10*D*, *left*, blue line). Indeed, these gradual rises were comparable to those that did precede spikes (Fig. 10*D*, *left*, red line; 38.08–170.03 ms, 20th–80th percentiles, median 89.10 ms; $P = 0.0267$, rank sum test, greater than the Bonferroni-corrected P value of 0.017 for 3 comparisons, $n = 263$ depolarizing events with a spike in the current neuron and 211 depolarizing events with no spikes in the current neuron but a spike in the nearby neuron from 7 cell pairs in barrel cortex). The amplitudes of the gradual rises followed a similar pattern (Fig. 10*D*, *right*), although the gradual rise was smaller in the cell that did not fire (shown in Fig. 10*F*).

If the gradual rises indeed represent a form of brief activated state shared across subsets of neurons, the ramp-ups (which, as defined above, include both the gradual rise and subsequent fast-rise components) would be expected to begin relatively synchronously. To determine if this was the case, we computed the start of the ramp-up in each cell on the basis of when that cell's membrane potential went and stayed above baseline until spike threshold was reached in the spiking cell of the pair: 16.8% of ramp-ups started within 10 ms of each other, 36.0% started within 20 ms of each other, and start times were correlated (Fig. 10*E*; $P < 10^{-10}$, Pearson's linear correlation coefficient $r = 0.389$, $n = 249$ spikes). In contrast to the coordination of gradual rises across multiple neurons, fast rises were cell specific: when one neuron spiked and the other did not, the spiking neuron had a fast rise of amplitude 2.93–13.95 mV (20th–80th percentiles, median 5.98 mV), whereas in the nonspiking cell, the change in voltage was essentially absent at 0–1.89 mV (20th–80th percentiles, median 0.06 mV; Fig. 10*G*). Thus, unlike the shared gradual rises that appeared in multiple neurons in the network, fast rises may reflect inputs specific to individual cells or small subsets of cells in the network.

If spiking was highly correlated across neurons, it would in principle be possible that gradual rises might appear correlated simply because they preceded correlated spikes. However, consistent with what others have reported (e.g., Poulet and Petersen 2008), spiking rarely occurred within a short time window in both neurons of a recorded pair. Of 7 pairs, only one had spikes co-occurring within 50 ms across the 2 cells. In general, spikes co-occurring within hundreds of milliseconds were few, and in our analysis we therefore pooled all spikes (i.e., co-occurring as well as non-co-occurring). Analysis of cases in which both cells spiked within 150 ms showed the same qualitative pattern as over the entire spike population. We also performed the same analysis including only cases when one cell spiked but the other one did not, and again obtained similar results (Fig. 10, *E–G*).

Others have observed highly correlated membrane potentials across simultaneously recorded cells during periods of quiescence lasting for seconds (Lampl et al. 1999; Poulet and Petersen 2008). During these highly correlated states, prominent 3- to 5-Hz oscillations were also observed in membrane potential. We wondered if the correlated ramp-ups we found could simply be a result of these highly correlated periods, which might last for periods of time longer than the ramp-ups themselves. If that were the case, we might expect to see periods of correlated membrane potential flanking the ramp-ups. To determine if correlated ramp-ups fell within such correlated network states, we analyzed membrane potential correlations during the period immediately preceding spikes, both when ramp-ups occur (15–215 ms before the spike) and in the preceding period before the ramp-up (an equivalent time period immediately beforehand). Comparing highly correlated ramp-up periods (correlation >0.8) and decorrelated ramp-ups periods (correlation <0.2), we found no significant difference in the membrane potential correlations immediately preceding those ramp-up periods ($P > 0.7$, Kolmogorov-Smirnov test; Fig. 11, *A* and *B*). Thus highly correlated ramp-ups were not simply part of longer periods of more highly correlated network states, although the ramp-ups could potentially be part of shorter network-wide states.

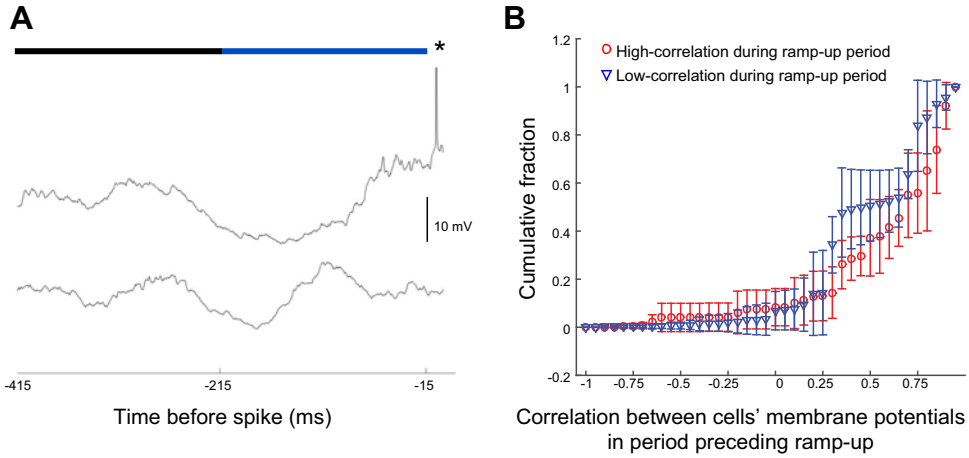

Fig. 11. Membrane potential correlations of 2 simultaneously patched cells change over short timescales. *A*: sample traces of 2 simultaneously patched neurons, illustrating the 2 periods analyzed, 415–215 ms before the spike (horizontal black bar above traces) and 215–15 ms before the spike (horizontal blue bar above traces). Asterisk indicates cropped spike. In this example, the cells were highly correlated during the period before the ramp-up (black bar) but not during the ramp-up (blue bar). *B*: cumulative distribution of membrane potential correlations before a ramp-up (415–215 ms before a spike) for ramp-ups that had a low (<0.2; blue) or high (>0.8; red) membrane potential correlation between the cells (215–15 ms before the spike). The 2 distributions are not significantly different ($P > 0.7$, Kolmogorov-Smirnov test; $n = 4$ pairs of simultaneously recorded neurons, each with at least 5 high- and 5 low-correlation ramp-up periods).

DISCUSSION

We have shown, using an awake animal-optimized version of our previously published autopatching robot (Kodandaramaiah et al. 2012, 2016), as well as using a four-patch version capable of recording multiple cells at once, and recording in both the hippocampus and the barrel cortex of awake mice, that in both brain regions spikes are nearly always preceded by two distinct subthreshold voltage changes: a fast (4–17 ms) monotonic rise in membrane voltage that brings the neuron above threshold, riding on top of a slower (tens to hundreds of milliseconds) gradual depolarization from baseline. The amplitude of the gradual voltage rises was ~3–10 mV, similar to other subthreshold events known to modulate spike probability (Carandini and Ferster 2000; Contreras and Palmer 2003; Haider et al. 2007; Sanchez-Vives and McCormick 2000). In support of this hypothesis, we found that such depolarizing ramps facilitate spike probability when assessed with brief current injections near threshold. Importantly, neurons were much more likely to spike in response to a brief injected current if it was preceded by a gradual rise, and the probability of spiking was higher for longer gradual rises compared with shorter rises that reached the same prestimulus voltage above baseline. Therefore, the correlation between ramp duration and increased spike probability was not simply due to patterns of activity in the network that drive both spiking and long ramp-ups. Instead, long ramp-ups increase spike probability in a cell-specific manner. Using dual patch recordings in the barrel cortex, we found that whereas the fast component was highly cell specific, the gradual component was shared across multiple neurons in the network. This correlation between cells during gradual rises was not simply due to long periods of correlated activity across cells: we found that correlations between cells could change over the course of hundreds of milliseconds and that membrane potential correlations during periods before correlated ramp-ups were similar to those before decorrelated ramp-ups.

In the hippocampus, where much work has focused on how neural codes are influenced by various rhythms, these gradual rises occurred independently of behavioral state and LFP oscillatory state (e.g., periods of theta or sharp-wave ripple) and were themselves aperiodic, suggesting that gradual rises were not simply intracellular correlates of classical neural oscillations. Furthermore, there was no prominent LFP signature associated with gradual rises, suggesting that the fraction of neurons engaged during such a rise was potentially much lower than found in states (e.g., up/down states) associated with prominent LFP events. Thus gradual rises may represent a "mesoscale" activated state, with intermediate durations, and likely intermediate numbers of neurons, compared with other states commonly studied that are present in a variety of network and behavioral states, in multiple brain regions. In support of this, although we often saw correlations between gradual rises across neurons in a simultaneously recorded pair in barrel cortex, neurons' membrane dynamics were often not correlated, or even anticorrelated (see Fig. 10*A*), suggesting that the ensemble of neurons engaged by any one ramp event is a fraction of the neurons in the microcircuit, and the ensemble engaged by a particular ramp event can be dynamically selected.

Duration of the Mesoscale Activated States Affects Spiking Probability Independently of Peak Voltage

In both barrel cortex and hippocampus, the GLM derived from the experimental data shows that, for a given amplitude, spiking probability significantly increases with duration of the mesoscale activated state. This is in contrast to the behavior shown by a simplified model, which assumes exponentially distributed gradual rise durations and fast inputs arriving on a Poisson schedule. Both single-neuron and network-level mechanisms could explain this unexpected finding. At the single-neuron level, for example, the relatively prolonged depolarization might prime the neuron to be more responsive to incoming inputs. One possibility is that slow depolarization could enhance persistent sodium current, known to be present in hippocampal and cortical pyramidal neurons (Crill 1996), to augment depolarization upon synaptic input (Schwindt and Crill 1995; Stafstrom et al. 1982, 1985). Our finding could, in principle, also be explained by postulating different combinations of gradual rise and fast input distributions. For example, this could happen if the fast inputs do not, in fact, follow a Poisson schedule, but their instantaneous probability increases as a function of time elapsed since the last one. One way to test this is to use exogenously delivered stimuli, because they do not affect the probability and schedule of fast inputs received by the neuron during a gradual rise. As shown in Fig. 6, the correlation between longer gradual rises and increased firing probability is observed for such stimulation, as well, suggesting that single-cell effects play an important role. Although we cannot confirm the identity of every recorded cell, we expect almost all of the recordings to have been made in pyramidal cells. Two cells in CA1 and three cells in barrel cortex were filled with biocytin, as described in METHODS. In CA1, both cells were classified as pyramidal cells (see e.g., Fig. 1*D*, *left*), and in barrel cortex, two cells were classified as pyramidal cells (see e.g., Fig. 1*D*, *right*) and one cell as an interneuron on the basis of their morphology. This was in line with our expectations, on the basis of our prior recordings (Kodandaramaiah et al. 2012), and, for the CA1 recordings, because we were specifically targeting the CA1 stratum pyramidale.

Mesoscale Activated States and Previously Reported Subthreshold Dynamics

Several studies have analyzed subthreshold dynamics around spikes and across-cell coordination in anesthetized animals (Chen and Fetz 2005; Haider et al. 2010; Lampl et al. 1999) and in awake preparations (Bennett et al. 2013; Poulet and Petersen 2008). One key difference is that previous studies often focused on a very short time window (e.g., 20 ms) before the spike as being the prime determinant of spike generation (Chen and Fetz 2005; Poulet and Petersen 2008), generally paying less attention to the dynamics that brought the neuron from baseline to close to spike threshold. Yet, as we have shown, such dynamics play an important role in gating neuronal output. When slower dynamics have been discussed, these dynamics have mostly been characterized by their frequency content over relatively extended periods of time and correlations between cells across these frequencies (Bennett et al. 2013; Haider et al. 2010; Poulet and Petersen 2008; Yu and Ferster 2010). This approach would not detect how the correlation between subthreshold dynamics across neurons can

evolve over short timescales. Other previous studies have identified dynamic changes in membrane potential correlations over the timescale of seconds (e.g., Lampl et al. 1999), but whether such changes also occurred at shorter timescales had not, to the best of our knowledge, been investigated. We therefore suggest that a complementary, fruitful approach is to consider the gradual depolarizations on the 50- to 200-ms timescale described in the present article as individual "mesoscale" responsive, or activated states, shared by dynamically changing subsets of neurons in a network. Overall, our findings fit within the general theme of a rich variety of dynamics at multiple timescales emerging from many groups (Haider and McCormick 2009) and involving varying proportions of neurons within a network that jointly control spike generation in vivo. We presently bring into focus a set of neuronal states of intermediate durations and extent, which has hitherto not been explicitly recognized.

Possible Functional Implications of Mesoscale Activated States

At a theoretical level, such mesoscale activated states may have several effects that could be tested in the future using new technologies and specific behavioral contexts. Although assessing the possible role of mesoscale activated states in sensory responses was beyond the scope of the present article, the scheme we propose would be consistent with both the ability of neurons to respond rapidly to sensory stimulation (because of the fast rise) and with the large variability of responses shown in vivo (because whether the neuron fires in response to the fast barrage of inputs is determined by the presence or absence of a preexisting gradual rise).

Moreover, cell ensembles are often thought of as cells that fire together within a tight time window, which occur during many behavioral contexts and appear to reflect information highly relevant to the task at hand. By firing together in a coordinated fashion, such ensembles could drive any downstream cells receiving convergent input to fire more efficaciously (Börgers et al. 2005; Fries 2009). Mesoscale activated states might be a natural mechanism for facilitating the generation of such cell ensembles: gradual rises would prime a set of cells over tens of milliseconds so that when a network receives a barrage of input, these cells would be more likely to spike together.

Behaviorally, by making cells more likely to fire in response to subsequent inputs, mesoscale activated states could boost spiking to behaviorally relevant, but less salient, stimuli. Previous work has shown that spiking activity can increase during attention even in the absence of stimuli (Luck et al. 1997; Reynolds et al. 2000; Sundberg et al. 2009). One possibility is that the attentional state may boost activity even in the absence of stimuli because of such transient depolarizations as described in the present article; cells that enter mesoscale activated states would be perfectly poised to respond to stimuli, although also more likely to be driven above threshold by noise. It has been shown that when saccades occur, the visual cortex exhibits a transient increase in excitability (Rajkai et al. 2008) that lasts for a hundred milliseconds or so (as assessed with extracellular recording), raising the question of whether mechanisms like those described in our study may play a role. It may be of interest for future studies to explore the possible interactions between such mesoscale states and other postulated attentional mechanisms, such as gamma oscillations (Fries 2009; Womelsdorf et al. 2006).

Potential Cellular and Molecular Mechanisms

Further studies are needed to elucidate the cellular and network mechanisms that generate the mesoscale activated states described in the present article, but a starting point might be to first assess whether they are generated by any mechanisms engaged by, or similar to, those underlying classical oscillatory states. For example, up and down states are thought to arise from recurrent excitation between interconnected pyramidal cells that is controlled by feedback inhibition and that can have relatively rapid onset and offset as the network makes a transition as a whole (McCormick et al. 2003). Such whole network transitions are thought to require a high level of interconnectivity, which might apply to the barrel cortex, but not CA1 (at least considered in isolation), where connections between pyramidal cells are sparse (Shepherd 2004). Indeed, because the gradual rises were similar in appearance in two different brain regions, a tantalizing hypothesis is that there might be common cellular mechanisms at play in multiple distinct circuits. Although the connectivity patterns of neurons in CA1 and barrel cortex differ significantly, they share an inhibitory interneuronal circuit by which vasoactive intestinal peptide-positive (VIP+) interneurons inhibit pyramidal cell-targeting parvalbumin- (PV+) and somatostatin-positive (SOM+) interneurons, with the net effect that activating VIP+ interneurons disinhibits pyramidal cells in the network (Freund and Buzsáki 1996; Freund and Gulyás 1997; Markram et al. 2004; McBain and Fisahn 2001; Pi et al. 2013). Activating VIP+ interneurons in these circuits could result in the mesoscale activated states here described. A number of studies have already shown that activation of VIP+ interneurons in this circuit enables neuromodulators and glutamatergic projections (e.g., from higher order cortical regions) to drive local cortical depolarization (Fu et al. 2014; Lee et al. 2013; Pfeffer et al. 2013; Pi et al. 2013), suggesting these interneurons might be a common effector mechanism modulating excitability.

In the future, the ability to map neural circuits with both microcircuit detail and long-range projection capability (Chen et al. 2015; Petreanu et al. 2007), as well as new methods for intracellular recording or imaging of subthreshold events in many cells at once (Chen et al. 2013), may enable investigations of how the mesoscale events described arise from neural circuits.

APPENDIX: DERIVATION OF THE EQUATION FOR THE PROBABILITY OF SPIKING IN RESPONSE TO RAMPS OF DIFFERENT DURATIONS

Derivation of Eq. 1

T_R is the minimum of the independent, exponentially distributed random numbers T and τ. It is an elementary result of probability theory that then T_R is itself exponentially distributed with

$$E(T_R) = \frac{1}{\frac{1}{E(T)} + \frac{1}{E(\tau)}} = \frac{E(T)E(\tau)}{E(T) + E(\tau)}. \quad (2)$$

Furthermore,

$$P(\text{ramp ends in a spike}) = P[\min(T, \tau) = \tau] = P(\tau \le T), \quad (3)$$

and using again an elementary result of probability theory,

$$P(\tau \le T) = \frac{E(T)}{E(T) + E(\tau)}. \quad (4)$$

Combining Eqs. 3 and 4, we find

$$P(\text{ramp ends in a spike}) = \frac{E(T)}{E(T) + E(\tau)}, \quad (5)$$

If we suppose now that $T_0 > 0$, then

$$P(\text{ramp ends in a spike} \mid T_R \ge T_0) = P(\tau \le T \mid T \ge T_0 \text{ and } \tau \ge T_0).$$

Using the "lack of memory" property of exponentially distributed random variables, this conditional probability is the same as $P(\tau \le T)$, without the conditions $T \ge T_0$ and $\tau \ge T_0$. Using *Eq. 4*, we conclude

$$P(\text{ramp ends in a spike} \mid T_R \ge T_0) = \frac{E(T)}{E(T) + E(\tau)}. \quad (6)$$

Let $\epsilon > 0$. Because $T_0 > 0$ was arbitrary, we also have

$$P(\text{ramp ends in a spike} \mid T_R \ge T_0 + \epsilon) = \frac{E(T)}{E(T) + E(\tau)}. \quad (7)$$

Equations 6 and 7 imply

$$P(\text{ramp ends in a spike} \mid T_0 \le T_R < T_0 + \epsilon) = \frac{E(T)}{E(T) + E(\tau)}.$$

Taking the limit as $\epsilon \to 0$, and using *Eq. 2*, we obtain *Eq. 1*.

ACKNOWLEDGMENTS

We thank Sunanda Sharma, Melina Tsitsiklis, Ilya Kolb, Denis Bozic, and Sean Batir for training animals and setting up the VR system.

GRANTS

A. C. Singer was funded by the MIT Intelligence Initiative. G. Talei Franzesi was funded by a Friends of the McGovern Institute Fellowship. E. S. Boyden was funded by NIH Director's Pioneer Award 1DP1NS087724 and Transformative Award 1R01MH103910-01, a New York Stem Cell Foundation-Robertson Award, the Cognitive Rhythms Collaborative funded by NSF DMS 1042134, and NIH Grants 1R01EY023173, 1R01NS067199, and 1R01DA029639. C. Borgers and N. J. Kopell were funded by NIH Grant 1R01 NS067199. S. B. Kodandaramaiah received financial remuneration from Neuromatic Devices for technical consulting services.

DISCLOSURES

No conflicts of interest, financial or otherwise, are declared by the authors.

AUTHOR CONTRIBUTIONS

A.C.S., G.T.F., S.B.K., C.B., C.R.F., N.J.K., and E.S.B. conceived and designed research; A.C.S., G.T.F., S.B.K., F.J.F., J.D.C., and A.K.L. performed experiments; A.C.S., G.T.F., and C.B. analyzed data; A.C.S., G.T.F., C.B., and E.S.B. interpreted results of experiments; A.C.S. and G.T.F. prepared figures; A.C.S., G.T.F., C.B., and E.S.B. drafted manuscript; A.C.S., G.T.F., and E.S.B. edited and revised manuscript; A.C.S., G.T.F., S.B.K., F.J.F., J.D.C., A.K.L., C.B., C.R.F., N.J.K., and E.S.B. approved final version of manuscript.

REFERENCES

Andersen P. *The Hippocampus Book*. Oxford: Oxford University Press, 2007.

Aronov D, Tank DW. Engagement of neural circuits underlying 2D spatial navigation in a rodent virtual reality system. *Neuron* 84: 442–456, 2014. doi:10.1016/j.neuron.2014.08.042.

Azouz R, Gray CM. Dynamic spike threshold reveals a mechanism for synaptic coincidence detection in cortical neurons in vivo. *Proc Natl Acad Sci USA* 97: 8110–8115, 2000. doi:10.1073/pnas.130200797.

Azouz R, Gray CM. Adaptive coincidence detection and dynamic gain control in visual cortical neurons in vivo. *Neuron* 37: 513–523, 2003. doi:10.1016/S0896-6273(02)01186-8.

Azouz R, Gray CM. Stimulus-selective spiking is driven by the relative timing of synchronous excitation and disinhibition in cat striate neurons in vivo. *Eur J Neurosci* 28: 1286–1300, 2008. doi:10.1111/j.1460-9568.2008.06434.x.

Başar E, Başar-Eroglu C, Karakaş S, Schürmann M. Gamma, alpha, delta, and theta oscillations govern cognitive processes. *Int J Psychophysiol* 39: 241–248, 2001. doi:10.1016/S0167-8760(00)00145-8.

Bean BP. The action potential in mammalian central neurons. *Nat Rev Neurosci* 8: 451–465, 2007. doi:10.1038/nrn2148.

Bennett C, Arroyo S, Hestrin S. Subthreshold mechanisms underlying state-dependent modulation of visual responses. *Neuron* 80: 350–357, 2013. doi:10.1016/j.neuron.2013.08.007.

Börgers C, Epstein S, Kopell NJ. Background gamma rhythmicity and attention in cortical local circuits: a computational study. *Proc Natl Acad Sci USA* 102: 7002–7007, 2005. doi:10.1073/pnas.0502366102.

Buzsáki G. Theta oscillations in the hippocampus. *Neuron* 33: 325–340, 2002. doi:10.1016/S0896-6273(02)00586-X.

Buzsáki G. *Rhythms of the Brain*. Oxford: Oxford University Press, 2006. doi:10.1093/acprof:oso/9780195301069.001.0001

Buzsáki G, Buhl DL, Harris KD, Csicsvari J, Czéh B, Morozov A. Hippocampal network patterns of activity in the mouse. *Neuroscience* 116: 201–211, 2003. doi:10.1016/S0306-4522(02)00669-3.

Buzsáki G, Draguhn A. Neuronal oscillations in cortical networks. *Science* 304: 1926–1929, 2004. doi:10.1126/science.1099745.

Carandini M, Ferster D. Membrane potential and firing rate in cat primary visual cortex. *J Neurosci* 20: 470–484, 2000.

Carr MF, Jadhav SP, Frank LM. Hippocampal replay in the awake state: a potential substrate for memory consolidation and retrieval. *Nat Neurosci* 14: 147–153, 2011. doi:10.1038/nn.2732.

Chen D, Fetz EE. Characteristic membrane potential trajectories in primate sensorimotor cortex neurons recorded in vivo. *J Neurophysiol* 94: 2713–2725, 2005. doi:10.1152/jn.00024.2005.

Chen F, Tillberg PW, Boyden ES. Expansion microscopy. *Science* 347: 543–548, 2015. doi:10.1126/science.1260088.

Chen TW, Wardill TJ, Sun Y, Pulver SR, Renninger SL, Baohan A, Schreiter ER, Kerr RA, Orger MB, Jayaraman V, Looger LL, Svoboda K, Kim DS. Ultrasensitive fluorescent proteins for imaging neuronal activity. *Nature* 499: 295–300, 2013. doi:10.1038/nature12354.

Contreras D, Palmer L. Response to contrast of electrophysiologically defined cell classes in primary visual cortex. *J Neurosci* 23: 6936–6945, 2003.

Crill WE. Persistent sodium current in mammalian central neurons. *Annu Rev Physiol* 58: 349–362, 1996. doi:10.1146/annurev.ph.58.030196.002025.

Csicsvari J, Hirase H, Czurkó A, Mamiya A, Buzsáki G. Oscillatory coupling of hippocampal pyramidal cells and interneurons in the behaving Rat. *J Neurosci* 19: 274–287, 1999.

Davidson TJ, Kloosterman F, Wilson MA. Hippocampal replay of extended experience. *Neuron* 63: 497–507, 2009. doi:10.1016/j.neuron.2009.07.027.

Dragoi G, Tonegawa S. Preplay of future place cell sequences by hippocampal cellular assemblies. *Nature* 469: 397–401, 2011. doi:10.1038/nature09633.

Epsztein J, Brecht M, Lee AK. Intracellular determinants of hippocampal CA1 place and silent cell activity in a novel environment. *Neuron* 70: 109–120, 2011. doi:10.1016/j.neuron.2011.03.006.

Fontaine B, Peña JL, Brette R. Spike-threshold adaptation predicted by membrane potential dynamics in vivo. *PLOS Comput Biol* 10: e1003560, 2014. doi:10.1371/journal.pcbi.1003560.

Foster DJ, Wilson MA. Reverse replay of behavioural sequences in hippocampal place cells during the awake state. *Nature* 440: 680–683, 2006. doi:10.1038/nature04587.

Fox J. *Applied Regression Analysis and Generalized Linear Models*. Thousand Oaks, CA: Sage, 2008.

Freund TF, Buzsáki G. Interneurons of the hippocampus. *Hippocampus* 6: 347–470, 1996. doi:10.1002/(SICI)1098-1063(1996)6:4<347::AID-HIPO1>3.0.CO;2-I.

Freund TF, Gulyás AI. Inhibitory control of GABAergic interneurons in the hippocampus. *Can J Physiol Pharmacol* 75: 479–487, 1997. doi:10.1139/y97-033.

Fries P. Neuronal gamma-band synchronization as a fundamental process in cortical computation. *Annu Rev Neurosci* 32: 209–224, 2009. doi:10.1146/annurev.neuro.051508.135603.

Fu Y, Tucciarone JM, Espinosa JS, Sheng N, Darcy DP, Nicoll RA, Huang ZJ, Stryker MP. A cortical circuit for gain control by behavioral state. *Cell* 156: 1139–1152, 2014. doi:10.1016/j.cell.2014.01.050.

Grienberger C, Chen X, Konnerth A. NMDA receptor-dependent multidendrite Ca^{2+} spikes required for hippocampal burst firing in vivo. *Neuron* 81: 1274–1281, 2014. doi:10.1016/j.neuron.2014.01.014.

Guo ZV, Hires SA, Li N, O'Connor DH, Komiyama T, Ophir E, Huber D, Bonardi C, Morandell K, Gutnisky D, Peron S, Xu NL, Cox J, Svoboda K. Procedures for behavioral experiments in head-fixed mice. *PLoS One* 9: e88678, 2014. doi:10.1371/journal.pone.0088678.

Haider B, Duque A, Hasenstaub AR, McCormick DA. Neocortical network activity in vivo is generated through a dynamic balance of excitation and inhibition. *J Neurosci* 26: 4535–4545, 2006. doi:10.1523/JNEUROSCI.5297-05.2006.

Haider B, Duque A, Hasenstaub AR, Yu Y, McCormick DA. Enhancement of visual responsiveness by spontaneous local network activity in vivo. *J Neurophysiol* 97: 4186–4202, 2007. doi:10.1152/jn.01114.2006.

Haider B, Krause MR, Duque A, Yu Y, Touryan J, Mazer JA, McCormick DA. Synaptic and network mechanisms of sparse and reliable visual cortical activity during nonclassical receptive field stimulation. *Neuron* 65: 107–121, 2010. doi:10.1016/j.neuron.2009.12.005.

Haider B, McCormick DA. Rapid neocortical dynamics: cellular and network mechanisms. *Neuron* 62: 171–189, 2009. doi:10.1016/j.neuron.2009.04.008.

Harris KD, Hirase H, Leinekugel X, Henze DA, Buzsáki G. Temporal interaction between single spikes and complex spike bursts in hippocampal pyramidal cells. *Neuron* 32: 141–149, 2001. doi:10.1016/S0896-6273(01)00447-0.

Hartigan JA, Hartigan PM. The dip test of unimodality. *Ann Stat* 13: 70–84, 1985. doi:10.1214/aos/1176346577.

Harvey CD, Collman F, Dombeck DA, Tank DW. Intracellular dynamics of hippocampal place cells during virtual navigation. *Nature* 461: 941–946, 2009. doi:10.1038/nature08499.

Henze DA, Buzsáki G. Action potential threshold of hippocampal pyramidal cells in vivo is increased by recent spiking activity. *Neuroscience* 105: 121–130, 2001. doi:10.1016/S0306-4522(01)00167-1.

Hirase H, Leinekugel X, Czurkó A, Csicsvari J, Buzsáki G. Firing rates of hippocampal neurons are preserved during subsequent sleep episodes and modified by novel awake experience. *Proc Natl Acad Sci USA* 98: 9386–9390, 2001. doi:10.1073/pnas.161274398.

Klimesch W. EEG alpha and theta oscillations reflect cognitive and memory performance: a review and analysis. *Brain Res Brain Res Rev* 29: 169–195, 1999. doi:10.1016/S0165-0173(98)00056-3.

Kodandaramaiah SB, Franzesi GT, Chow BY, Boyden ES, Forest CR. Automated whole-cell patch-clamp electrophysiology of neurons in vivo. *Nat Methods* 9: 585–587, 2012. doi:10.1038/nmeth.1993.

Kodandaramaiah SB, Holst GL, Wickersham IR, Singer AC, Franzesi GT, McKinnon ML, Forest CR, Boyden ES. Assembly and operation of the autopatcher for automated intracellular neural recording in vivo. *Nat Protoc* 11: 634–654, 2016. doi:10.1038/nprot.2016.007.

Lampl I, Reichova I, Ferster D. Synchronous membrane potential fluctuations in neurons of the cat visual cortex. *Neuron* 22: 361–374, 1999. doi:10.1016/S0896-6273(00)81096-X.

Lee AK, Epsztein J, Brecht M. Head-anchored whole-cell recordings in freely moving rats. *Nat Protoc* 4: 385–392, 2009. doi:10.1038/nprot.2009.5.

Lee AK, Epsztein J, Brecht M. Whole-cell patch-clamp recordings in freely moving animals. In: Patch-Clamp Methods and Protocols (2nd ed.), edited by Martina M and Taverna S. New York: Humana, 2014, p. 263–276.

Lee S, Kruglikov I, Huang ZJ, Fishell G, Rudy B. A disinhibitory circuit mediates motor integration in the somatosensory cortex. *Nat Neurosci* 16: 1662–1670, 2013. doi:10.1038/nn.3544.

Luck SJ, Chelazzi L, Hillyard SA, Desimone R. Neural mechanisms of spatial selective attention in areas V1, V2, and V4 of macaque visual cortex. *J Neurophysiol* 77: 24–42, 1997.

Mainen ZF, Sejnowski TJ. Reliability of spike timing in neocortical neurons. *Science* 268: 1503–1506, 1995. doi:10.1126/science.7770778.

Markram H, Toledo-Rodriguez M, Wang Y, Gupta A, Silberberg G, Wu C. Interneurons of the neocortical inhibitory system. *Nat Rev Neurosci* 5: 793–807, 2004. doi:10.1038/nrn1519.

McBain CJ, Fisahn A. Interneurons unbound. *Nat Rev Neurosci* 2: 11–23, 2001. doi:10.1038/35049047.

McCormick DA, Shu Y, Hasenstaub A, Sanchez-Vives M, Badoual M, Bal T. Persistent cortical activity: mechanisms of generation and effects on neuronal excitability. *Cereb Cortex* 13: 1219–1231, 2003. doi:10.1093/cercor/bhg104.

McGinley MJ, David SV, McCormick DA. Cortical membrane potential signature of optimal states for sensory signal detection. *Neuron* 87: 179–192, 2015b. doi:10.1016/j.neuron.2015.05.038.

McGinley MJ, Vinck M, Reimer J, Batista-Brito R, Zagha E, Cadwell CR, Tolias AS, Cardin JA, McCormick DA. Waking State: Rapid Variations Modulate Neural and Behavioral Responses. *Neuron* 87: 1143–1161, 2015a. doi:10.1016/j.neuron.2015.09.012.

Nelder JA, Wedderburn RWM. Generalized linear models. In: *Breakthroughs in Statistics*, edited by Kotz S and Johnson NL. New York: Springer, 1992, p. 547–563. doi:10.1007/978-1-4612-4380-9_39

Nowak LG, Sanchez-Vives MV, McCormick DA. Influence of low and high frequency inputs on spike timing in visual cortical neurons. *Cereb Cortex* 7: 487–501, 1997. doi:10.1093/cercor/7.6.487.

Petreanu L, Huber D, Sobczyk A, Svoboda K. Channelrhodopsin-2-assisted circuit mapping of long-range callosal projections. *Nat Neurosci* 10: 663–668, 2007. doi:10.1038/nn1891.

Pfeffer CK, Xue M, He M, Huang ZJ, Scanziani M. Inhibition of inhibition in visual cortex: the logic of connections between molecularly distinct interneurons. *Nat Neurosci* 16: 1068–1076, 2013. doi:10.1038/nn.3446.

Pi HJ, Hangya B, Kvitsiani D, Sanders JI, Huang ZJ, Kepecs A. Cortical interneurons that specialize in disinhibitory control. *Nature* 503: 521–524, 2013. doi:10.1038/nature12676.

Pouille F, Scanziani M. Enforcement of temporal fidelity in pyramidal cells by somatic feed-forward inhibition. *Science* 293: 1159–1163, 2001. doi:10.1126/science.1060342.

Poulet JF, Petersen CC. Internal brain state regulates membrane potential synchrony in barrel cortex of behaving mice. *Nature* 454: 881–885, 2008. doi:10.1038/nature07150.

Rajkai C, Lakatos P, Chen C-M, Pincze Z, Karmos G, Schroeder CE. Transient cortical excitation at the onset of visual fixation. *Cereb Cortex* 18: 200–209, 2008. doi:10.1093/cercor/bhm046.

Ravassard P, Kees A, Willers B, Ho D, Aharoni D, Cushman J, Aghajan ZM, Mehta MR. Multisensory control of hippocampal spatiotemporal selectivity. *Science* 340: 1342–1346, 2013. doi:10.1126/science.1232655.

Reimer J, Froudarakis E, Cadwell CR, Yatsenko D, Denfield GH, Tolias AS. Pupil fluctuations track fast switching of cortical states during quiet wakefulness. *Neuron* 84: 355–362, 2014. doi:10.1016/j.neuron.2014.09.033.

Reynolds JH, Pasternak T, Desimone R. Attention increases sensitivity of V4 neurons. *Neuron* 26: 703–714, 2000. doi:10.1016/S0896-6273(00)81206-4.

Sanchez-Vives MV, McCormick DA. Cellular and network mechanisms of rhythmic recurrent activity in neocortex. *Nat Neurosci* 3: 1027–1034, 2000. doi:10.1038/79848.

Schwindt PC, Crill WE. Amplification of synaptic current by persistent sodium conductance in apical dendrite of neocortical neurons. *J Neurophysiol* 74: 2220–2224, 1995.

Seelig JD, Chiappe ME, Lott GK, Dutta A, Osborne JE, Reiser MB, Jayaraman V. Two-photon calcium imaging from head-fixed *Drosophila* during optomotor walking behavior. *Nat Methods* 7: 535–540, 2010. doi:10.1038/nmeth.1468.

Shepherd GM, editor. *The Synaptic Organization of the Brain*. New York: Oxford University Press, 2004. doi:10.1093/acprof:oso/9780195159561.001.1

Singer W. Synchronization of cortical activity and its putative role in information processing and learning. *Annu Rev Physiol* 55: 349–374, 1993. doi:10.1146/annurev.ph.55.030193.002025.

Stafstrom CE, Schwindt PC, Chubb MC, Crill WE. Properties of persistent sodium conductance and calcium conductance of layer V neurons from cat sensorimotor cortex in vitro. *J Neurophysiol* 53: 153–170, 1985.

Stafstrom CE, Schwindt PC, Crill WE. Negative slope conductance due to a persistent subthreshold sodium current in cat neocortical neurons in vitro. *Brain Res* 236: 221–226, 1982. doi:10.1016/0006-8993(82)90050-6.

Steriade M, McCormick DA, Sejnowski TJ. Thalamocortical oscillations in the sleeping and aroused brain. *Science* 262: 679–685, 1993. doi:10.1126/science.8235588.

Steriade M, Timofeev I, Grenier F. Natural waking and sleep states: a view from inside neocortical neurons. *J Neurophysiol* 85: 1969–1985, 2001.

Sundberg KA, Mitchell JF, Reynolds JH. Spatial attention modulates center-surround interactions in macaque visual area v4. *Neuron* 61: 952–963, 2009. doi:10.1016/j.neuron.2009.02.023.

Womelsdorf T, Fries P, Mitra PP, Desimone R. Gamma-band synchronization in visual cortex predicts speed of change detection. *Nature* 439: 733–736, 2006. doi:10.1038/nature04258.

Ylinen A, Bragin A, Nádasdy Z, Jandó G, Szabó I, Sik A, Buzsáki G. Sharp wave-associated high-frequency oscillation (200 Hz) in the intact hippocampus: network and intracellular mechanisms. *J Neurosci* 15: 30–46, 1995.

Yu J, Ferster D. Membrane potential synchrony in primary visual cortex during sensory stimulation. *Neuron* 68: 1187–1201, 2010. doi:10.1016/j.neuron.2010.11.027.

Zagha E, McCormick DA. Neural control of brain state. *Curr Opin Neurobiol* 29: 178–186, 2014. doi:10.1016/j.conb.2014.09.010.